Check for updates

Recent progress in Zn-based anodes for advanced lithium ion batteries

Lei Wang, [a] Guanhua Zhang, [*ab] Quanhui Liu[c] and Huigao Duan[ab]

Developing high-performance anode materials is essential for advanced next-generation lithium ion batteries. ZnO-based nanomaterials have been considered promising candidates owing to their high theoretical specific capacity, environmental friendliness, and relatively low cost. However, major problems, including inherent poor conductivity and huge volume expansion, have severely impeded ZnO-based nanomaterials from being viable. Here, we first present a brief review of the most effective strategies to improve the lithium ion storage performance of ZnO-based anodes. In addition, recent advances in other novel Zn-based nanomaterials are also summarized and discussed. Finally, we describe the challenges and prospects of future research trends for Zn-based nanomaterials.
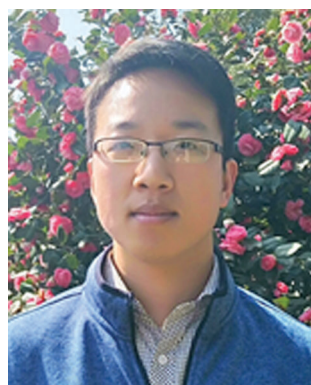
1. Introduction

Renewable energy sources such as solar energy, wind and waves have attracted enormous attention to address the shortage of fossil fuels and the increasingly serious environmental issues.[1,2] However, without effective energy storage and conversion

[a] State Key Laboratory of Advanced Design and Manufacturing for Vehicle Body, School of Physics and Electronics, Hunan University, Changsha, 410082, P. R. China. E-mail: guanhuazhang@hnu.edu.cn

[b] National Engineering Research Center for High Efficiency Grinding, College of Mechanical and Vehicle Engineering, Hunan University, Changsha, 410082, P. R. China

[c] School of Physics and Electronics, Hunan University, Changsha, 410082, P. R. China

systems, these green energy sources cannot be widely used owing to their intermittent availability and their instability. In addition, high-performance energy storage and conversion devices are becoming more and more important for the rapid development of smart portable devices, electric vehicles (EVs) and hybrid electric vehicles (HEVs).[3–19] As one of the most important energy storage and conversion systems, lithium ion batteries (LIBs) have achieved wide commercial application owing to their high energy density, lack of memory effect, wide operating temperature range, long cycling life, and low self-discharge rate.[20,21] The electrodes (including anodes and cathodes) are the key components which will strongly affect the electrochemical performance of LIBs. For the anodes of LIBs, carbon-based materials, especially graphite, have played a crucial role since they were first introduced into

Lei Wang is a PhD candidate from the College of Physics and Electronics, Hunan University. His research interests include the design and synthesis of novel nanomaterials and their application in lithium ion batteries and supercapacitors.

Lei Wang

Guanhua Zhang received her PhD degree from Hunan University, P. R. China in 2016. From 2014 to 2016, she joined Arizona State University, as a visiting PhD student. Currently, she is an Associate Professor at the College of Mechanical and Vehicle Engineering, and a member of the State Key Laboratory of Advanced Design and Manufacturing for Vehicle Body, Hunan University, P. R. China. Her current research is focused on nanofabrication for energy conversion and storage (including lithium/sodium secondary batteries and supercapacitors), and electrocatalysis.

Guanhua Zhang

1414 | *Mater. Chem. Front.*, 2018, **2**, 1414–1435

This journal is © The Royal Society of Chemistry and the Chinese Chemical Society 2018

commercial LIBs by Sony in 1991. Nevertheless, the low theoretical capacity (372 mA h g^{-1}) and serious safety concerns greatly limit further practical applications of the graphite anode. In particular, an ever-increasing demand for power batteries with high energy density and high safety cannot be satisfied. Therefore, researchers are focusing on developing novel anode materials with high performance for next-generation LIBs.

Based on conversion reaction mechanism, nano-sized transition metal oxides (TMOs) deliver much higher theoretical specific capacity than the commercial carbon-based anodes.[22,23] Additionally, the higher lithiation potential of the TMOs can avoid the formation of lithium dendrites in the anodes, ensuring a better safety capability for LIBs. Among various TMOs, zinc oxide (ZnO) has been considered a promising anode material candidate for LIBs, benefiting from high theoretical specific capacity, environmental friendliness and low cost.[24] In addition, the low lithiation/delithiation potential of ZnO (lithiation potential *ca.* 0.5 V, delithiation potential 0–0.7 V and *ca.* 1.4 V) delivers an obvious advantage for high-output voltage and energy density.[25,26] Unfortunately, the huge volumetric change of ZnO during the Li ion interaction/extraction process usually causes severe pulverization and electrical disconnection between the active material and the current collector, leading to a dramatic decline of the cycling stability. In addition, the poor intrinsic electrical conductivity of ZnO is unfavorable for fast electron transport, limiting the rate capability of the ZnO anodes. Therefore, optimizing the nanostructure to improve the electrochemical performance of ZnO-based anodes is highly desirable.

Recently, various strategies have been developed to effectively improve the lithium ion storage performance of ZnO-based anodes. Despite a previous review outlining the structural design of ZnO-based anodes, a systematic summary of the different improvement approaches is of great importance. Under these circumstances, in this review we summarize the recently developed key approaches, in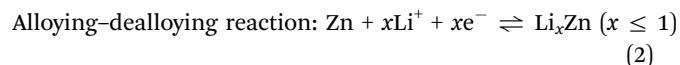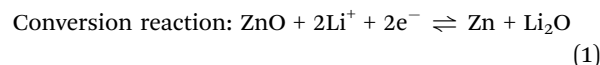cluding structure design, surface modification and component regulation, to enhance structure stability, ionic diffusion and electronic conductivity of ZnO-based anodes. In addition, other novel Zn-based nanomaterials such as ZnS, ZnSe, ZnP, ZnSb, and ZnTe are introduced. Finally, the future challenges and new opportunities of Zn-based anodes are outlined.

## 2. Synthetic methods for ZnO-based anodes

To date, various methods have been developed to synthesize ZnO nanostructures with controllable morphologies for lithium ion storage. According to the initial state of the reactive materials, the fabrication methods can be classified into solid-phase method, liquid-phase method and gas-phase method, as shown in Table 1.

3. Lithium ion storage mechanism of ZnO-based anodes

ZnO, as a typical TMO, delivers a high theoretical specific capacity by redox reaction in a multi-electron process. The electrochemical reaction mechanism of the ZnO anodes can be described as follows:[23,24]

$$\text{Conversion reaction: } ZnO + 2Li^+ + 2e^- \rightleftharpoons Zn + Li_2O \tag{1}$$

$$\text{Alloying–dealloying reaction: } Zn + xLi^+ + xe^- \rightleftharpoons Li_xZn \ (x \leq 1) \tag{2}$$

As the above equations represent, the Li ion storage mechanism of ZnO anodes includes two stages: conversion reaction to form Zn metal and Li$_2$O, and then alloying reaction to form lithium zinc alloy, accompanied by a multi-electron transfer process.
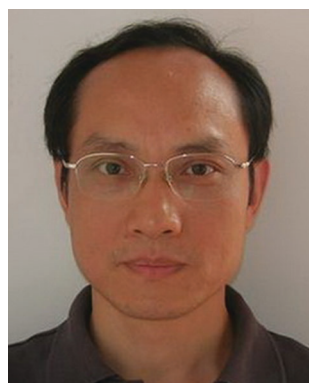
Quanhui Liu

Dr Professor Quanhui Liu (Q. H. Liu), Director of School for Theoretical Physics, Hunan University. Recent research interest focuses on quantum motion constrained on the hypersurface such as the nanostructure. He has resolved some important problems that were long believed intractable, such as construction of the fundamental commutation relations for the momentum, quantum conditions for inclusion of the geometric potential, and he identified the presence of the physical quantity, together with coining the terminology, geometric momentum.

Huigao Duan

Huigao Duan received his BSc degree (2004) and PhD (2010) in Condensed Matter Physics from Lanzhou University, P. R. China. He is currently a Professor at the College of Mechanical and Vehicle Engineering, and a member of the State Key Laboratory of Advanced Design and Manufacturing for Vehicle Body, Hunan University, P. R. China. From 2008 to 2010, he joined the Research Laboratory of Electronics, MIT, as a Visiting PhD Student. From 2010 to 2012, he worked as a staff Scientist in the Institute of Materials Research and Engineering, A*STAR in Singapore. His main research interests include sub-10 nm electron-beam lithography and its related applications in nanodevices.

This journal is © The Royal Society of Chemistry and the Chinese Chemical Society 2018

Mater. Chem. Front., 2018, **2**, 1414–1435 | **1415**

Table 1 Available synthetic methods for various ZnO nanostructures

Synthetic methods		ZnO nanostructures			
		0D (nanoparticle, nanosphere)	1D (nanorod, nanowire, nanofiber, nanotube, nanobelt)	2D (nanosheet, nanoplate, nanofilm, nanoflake, nanodisk)	3D (nanoflower, nanofoam, *et al.*)
Solid phase	Ball milling	✔	✔		
	Solid state reaction	✔	✔		
Liquid phase	Electro depositing	✔	✔	✔	✔
	Sol–gel	✔	✔	✔	✔
	Hydrothermal	✔	✔	✔	✔
	Solvothermal	✔	✔	✔	✔
	Electrospinning	✔	✔	✔	
	Precipitation	✔	✔	✔	✔
Gas phase	Magnetron sputtering	✔	✔	✔	
	Pulsed laser deposition	✔	✔	✔	
	Atomic layer deposition	✔		✔	
	Plasma chemical vapor deposition	✔	✔	✔	
	Thermal chemical vapor deposition	✔	✔	✔	

The theoretical specific capacity of ZnO anodes is related to the number of electrons transferred during the electrochemical reaction process and can be calculated according the following equation:

$$Q = \frac{nF}{3.6M_{w}} \qquad (3)$$

where Q is the gravimetric theoretical specific capacity (mA h g^{-1}), F is the Faraday constant (96 500 C mol^{-1}), n is the number of electrons transferred in the electrochemical reaction, and M_{w} is the molecular weight of active material (g mol^{-1}). As we can see from eqn (1) and (2), three electrons are transferred per mole of ZnO during the electrochemical reaction. Therefore, based on eqn (3), we can calculate a theoretical specific capacity of 987 mA h g^{-1}, which is almost twice that of graphite. This high theoretical specific capacity demonstrates that ZnO is a promising anode material for next-generation LIBs. However, the rapid capacity fading during cycling caused by a huge volume expansion (about 228%) is a big challenge of ZnO anodes. Moreover, the low inherent electrical conductivity of ZnO results in a limited rate performance. In order to overcome the above drawbacks and realize the practical application of ZnO-based anodes for next-generation batteries, lots of effective approaches have been developed to improve the battery performance. The recent key progress in designing and fabricating ZnO-based anodes with improved performance will be discussed in detail in this review.

4. Strategies for improving lithium ion storage performance

4.1 Nanostructure design

Poizot *et al.* first discovered that TMOs with nanostructure can be used as high-performance anode materials for LIBs in 2000.[27] Since then, numerous efforts have been devoted to this new research field.[28–31] Compared with the bulk materials, the novel nanostructured materials possess a series of unique advantages for the improved performance of the batteries. The nanoscale size can not only remarkably relieve the volume expansion to enhance the cycling capability, but also shorten the path distances of electron transfer and Li ion diffusion for better rate performance. Moreover, nanostructured materials with large specific surface areas are beneficial for providing more active sites to participate in the electrochemical energy storage reactions. Benefiting from the structural advantages, various nanostructured ZnO materials ranging from low to high dimensions have been designed and prepared as the anodes for LIBs with obviously enhanced electrochemical performance.

4.1.1 Zero-dimensional (0D) nanostructures. *In situ* study of the electrochemical behavior of ZnO nanoparticles during the lithiation reaction can be conducive to understanding the reaction mechanism for ZnO anodes. Su *et al.* investigated the lithium ion storage process of ZnO nanoparticles (25–45 nm) using *in situ* transmission electron microscopy (TEM) by constructing a nano-LIB based on an individual ZnO/graphene sheet electrode, as shown in Fig. 1a and b.[32] Two kinds of reaction modes were revealed which had different reaction rates, as illustrated in Fig. 1c. In the violent reaction mode, particles fractured into nanoparticle clusters within the Li$_2$O matrix in 1–2 min. During the peaceful evolution, the ZnO nanoparticle changed into core–shell particles consisting of Zn and LiZn nanograins. In addition, abnormally large Zn nanocrystals grew quickly in the violent reaction mode, which can suppress the formation of LiZn and result in rapid capacity decay. Recently, the partial recombination of ZnO during the charge reaction was found according to the results from a series of *ex situ* characterization technologies, which may be determined by the size of the Zn nanocrystallites formed by Li extraction from LiZn (Fig. 1d).[33] These results provide direct evidence and deep understanding of the lithiation reaction governing the performance of ZnO-based anodes.

Developing a facile and scalable method to prepare ZnO nanoparticles is extremely important to their practical
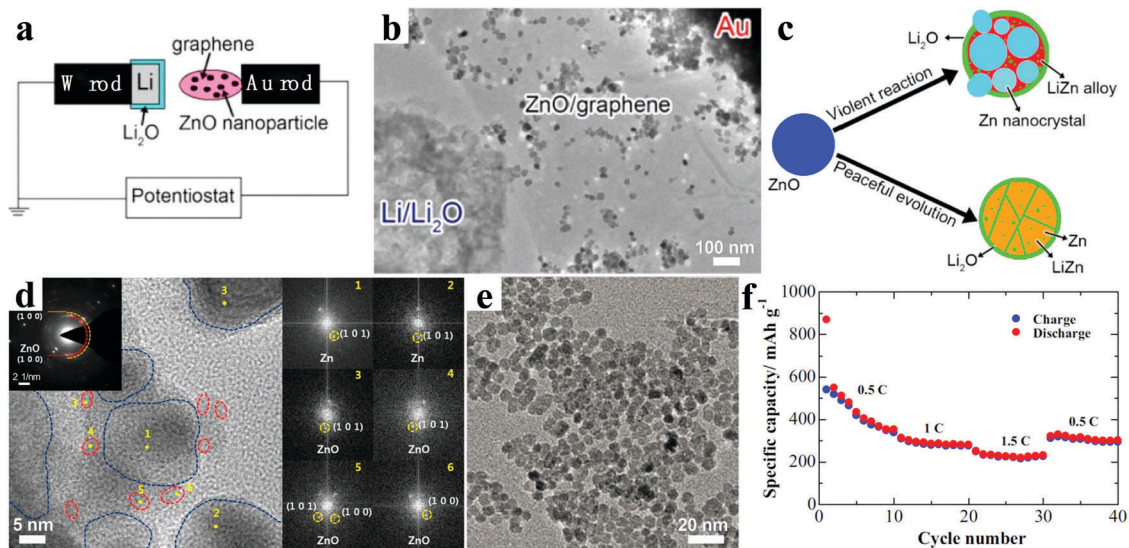
1416 | *Mater. Chem. Front.*, 2018, **2**, 1414–1435

This journal is © The Royal Society of Chemistry and the Chinese Chemical Society 2018

Fig. 1 (a) Schematic illustration and (b) TEM image of the *in situ* electrochemical nano-LIB constructed inside a TEM; (c) schematic illustration of the electrochemical reaction of ZnO with Li⁺. Reproduced with permission.[32] Copyright 2013, IOP Publishing Ltd. (d) High-resolution transmission electron microscopy (HRTEM) image of ZnO electrode at the fully charged state with the corresponding selected area electron diffraction (SAED) and Fourier transform (FT) patterns. Reproduced with permission.[33] Copyright 2016, Elsevier. (e) HRTEM image of the ZnO nanoparticles; (f) rate capability of lithium ion cells with the ZnO electrode. Reproduced with permission.[34] Copyright 2016, Springer.

application as LIB anode. Highly dispersed ZnO nanoparticles prepared by a versatile and scalable sol–gel synthetic technique were reported by Li *et al.*[34] According to Fig. 1e, the spherical ZnO nanoparticles obtained had an average size of only about 7 nm. Owing to the nano-size of the highly dispersed ZnO nanoparticles, outstanding electrochemical performance was demonstrated with a good rate capability of 229 mA h g⁻¹ at 1.5C (Fig. 1f).

4.1.2 One-dimensional (1D) nanostructures. Unfortunately, the 0D nanomaterials tend to aggregate due to high surface energy, resulting in capacity fading and slow kinetics. Besides, considerable contact resistance originating from multiple contact interfaces between active materials and binders or active materials and active materials also impairs the electrochemical performance. Compared with the 0D nanomaterials, 1D nanomaterials such as nanorods, nanowires and nanotubes, can alleviate these issues to some extent.

A series of 1D ZnO nanostructures were designed to further improve the performance of LIBs.[35–43] For example, Wang *et al.* prepared ZnO nanorod arrays with dandelion-like morphology directly grown on copper substrates by a facial hydrothermal method (Fig. 2a).[36] Compared with the bulk ZnO, the ZnO nanorod arrays showed superior electrochemical performance with a stable capacity after 40 cycles, which was about four times that of the bulk ZnO. Kundu *et al.* further reduced the size of ZnO nanorods *via* a simple chemical route (Fig. 2b).[37] The ZnO nanorod electrodes held a capacity of 230 mA h g⁻¹ after 100 cycles at 0.3C. The crystal structural evolution of a single ZnO nanowire electrode during the lithiation reaction was investigated by Kushima and co-workers.[38] They observed that the solid state amorphization in single-crystalline ZnO nanowires was mainly driven by nanocracking, as shown in
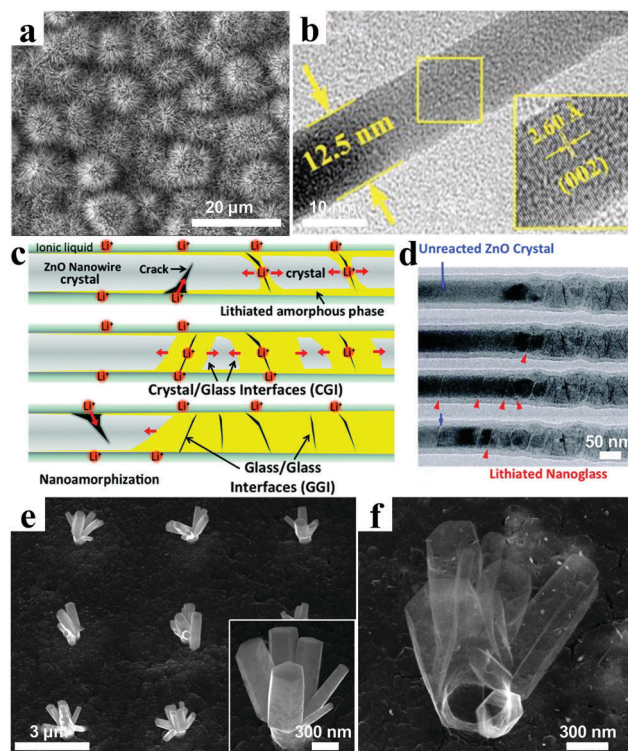

Fig. 2 (a) Scanning electron microscopy (SEM) image of the ZnO nanorod arrays. Reproduced with permission.[36] Copyright 2008, Elsevier. (b) HRTEM image of the ZnO nanorod. Reproduced with permission.[37] Copyright 2015, Elsevier. (c) Schematic illustration and (d) the corresponding TEM images explaining the leapfrog cracking and nanoamorphization lithiation mechanism of ZnO nanowires. Reproduced with permission.[38] Copyright 2011, American Chemical Society. SEM images of patterned arrays of ZnO nanorods (e) and nanotubes (f). Reproduced with permission.[40] Copyright 2012, American Chemical Society.

This journal is © The Royal Society of Chemistry and the Chinese Chemical Society 2018

Mater. Chem. Front., 2018, **2**, 1414–1435 | **1417**

Fig. 2c and d. Initially, in the crystalline nanowire, large tensile stresses near the surface induced by partial lithiation resulted in multiple nanocracking ahead of the main lithiation front, and the nanocracking penetrated the nanowire cross-section. Then, Li^{+} diffused and solid state amorphization occurred along the open crack surfaces. Finally, a glass–glass interface was left after the crack surfaces merged. In the divided segments, the same reaction also repeated, further pulverizing the nanowire into different nanoglass domains (nano-amorphization). These results provide useful guidance for developing promising ZnO electrode materials with regard to the crystal structure.

Based on the unique properties of the hollow nanostructures, ultrathin 1D ZnO nanotubes were introduced as the anodes for LIBs.[40] Pristine solid ZnO nanorods were synthesized by a simple hydrothermal method, as shown in Fig. 2e. Then the solid nanorods were spontaneously converted into ultrathin ZnO nanotubes in ambient NH_3 via a gas-phase chemical process, according to Fig. 2f. Owing to improved ion diffusion and effective alleviation of volume expansion, the ZnO nanotubes delivered a reversible capacity of 386 mA h g^{−1} at a current density of 0.5C after 50 cycles, which was about five times higher than that of the original ZnO nanorods (only 83 mA h g^{−1}).

4.1.3   Two-dimensional (2D) nanostructures. 2D nanomaterials have aroused increasing attention for high-performance LIBs owing to their high surface area and short ion diffusion paths. Fu and co-workers reported ZnO thin films were prepared by reactive pulsed laser deposition in ambient oxygen, and investigated the effect of the substrate temperature for fabricating as-deposited films on the electrochemical performance.[44] They found that highly textured crystalline ZnO films can be fabricated based on the optimal substrate temperature of about 500 °C (Fig. 3a). Based on ex situ TEM, they proposed a reaction mechanism including both the classical alloy and the

oxidation/reduction of nanoscale metal. Porous materials possess large electrode–electrolyte contact area and fast Li ion diffusion paths; thus they usually reveal enhanced electrochemical properties for LIBs. The combination of porosity and 2D nanostructure provides an effective approach for better electrochemical performance. For example, ZnO nanosheets with abundant mesopores were synthesized by two steps, comprising a simple homogeneous precipitation and a calcination process.[45] As shown in Fig. 3b, the nanosheets were assembled by interconnected nanostrips and formed a mesoporous net-like structure. The mesoporous ZnO nanosheets showed a first discharge capacity of 1070 mA h g^{−1} under a current density of 0.1 A g^{−1}, with an initial coulombic efficiency of about 60% (Fig. 3c). Recently, Wang et al. synthesized mesoporous ZnO nanosheets via a room temperature solvothermal method.[46] As seen from Fig. 3d, the nanosheets possessed a length of 1–2 μm and a thickness of 10–20 nm, and large mesopores were embedded in the walls of the nanosheets. The electrochemical results displayed a high specific capacity of 421 mA h g^{−1} after 100 cycles at 0.2 A g^{−1} and a good rate capability.

4.1.4   Three-dimensional (3D) nanostructures. Compared with lower-dimensional nanostructures, 3D nanostructures commonly exhibit more interspace to accommodate volume expansion and more active sites to accelerate lithium ion storage, resulting in excellent electrochemical stability and high rate capability.[47–53] Novel ZnO nanoflowers assembled from ultrathin nanosheets exhibited improved electrochemical properties compared with ZnO nanoplates owing to unique 3D structure features. Cauda et al. used a facile hydrothermal process to synthesize flower-like ZnO nanostructure, as shown in Fig. 4a.[48] With regard to lithium storage performance, it could exhibit a specific capacity of 175 mA h g^{−1} after 200 cycles at a reasonably high 1C rate, which was 42% of the initial reversible capacity at 0.2C (Fig. 4b). It is worth noting that such remarkable rate performance was obtained without introducing any foreign additives.

Other complex 3D structures also demonstrate their distinctive advantages. A bramble-like ZnO array was designed and successfully prepared through a facile two-step hydrothermal process.[50] The corresponding scanning electron microscopy image is shown in Fig. 4c. Meanwhile, the electrochemical properties of the bramble-like ZnO electrode were compared with those of the needle-like ZnO electrode. As shown in Fig. 4d, after 50 cycles, the bramble-like ZnO still retained a capacity of 782 mA h g^{−1} corresponding to 74% capacity retention, which was obviously higher than that of the needle-like ZnO with 67% capacity retention. The enhanced electrochemical performance of the bramble-like ZnO electrode mainly resulted from the nanorod subunits acting as "bridges" to connect the adjacent ZnO needles and providing extra active sites on the ZnO needles. Another typical 3D structure, hollow ZnO with radial morphology, was synthesized based on a polystyrene sphere template via a hydrothermal method; the TEM image of the sample is shown in Fig. 4e.[51] Good reproducibility and almost accordance in shape were found in the current–voltage (C–V) curves after the first cycle, indicating
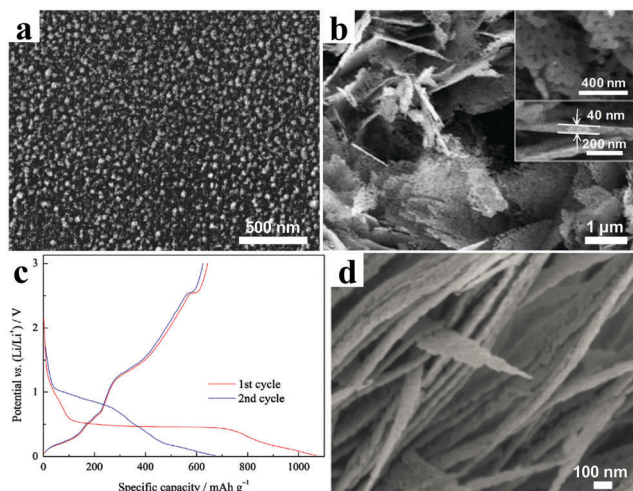

Fig. 3   (a) SEM image of the as-deposited ZnO at 500 °C. Reproduced with permission.[44] Copyright 2003, The Electrochemical Society. (b) SEM image of mesoporous ZnO nanosheets; (c) the first two charging/discharging curves of mesoporous ZnO nanosheets. Reproduced with permission.[45] Copyright 2014, Elsevier. (d) SEM image of the ZnO nanosheets. Reproduced with permission.[46] Copyright 2016, Springer.

1418 | Mater. Chem. Front., 2018, 2, 1414–1435

This journal is © The Royal Society of Chemistry and the Chinese Chemical Society 2018
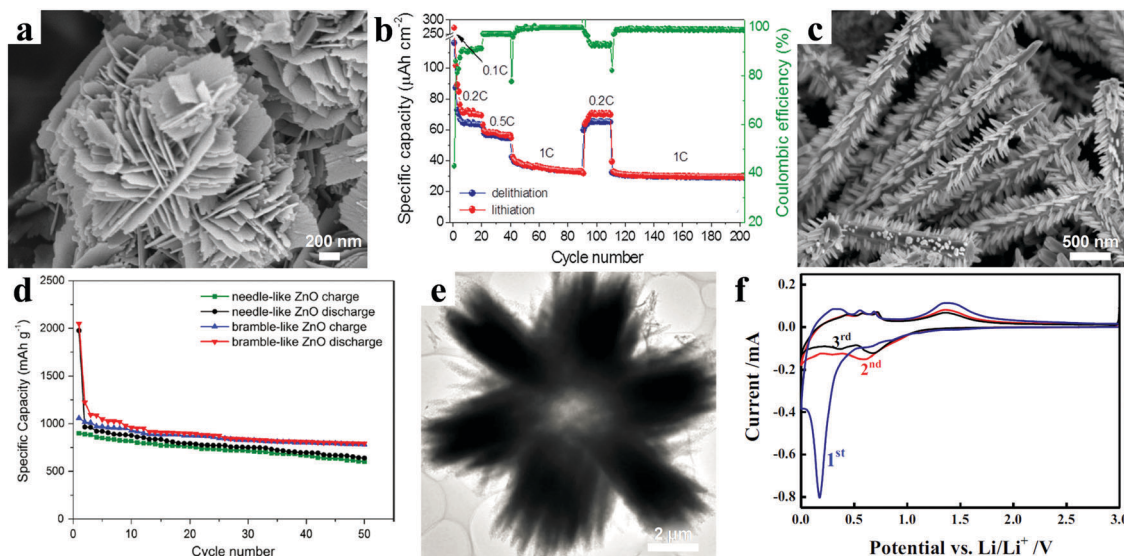
Fig. 4 (a) SEM image of the flower-like ZnO nanostructure; (b) rate performance at different current densities. Reproduced with permission.[48] Copyright 2013, Elsevier. (c) SEM image of the bramble-like ZnO arrays; (d) cycling performance of needle- and bramble-like ZnO electrodes. Reproduced with permission.[50] Copyright 2015, Springer. (e) TEM image of a radial ZnO microstructure; (f) CV curves of a hollow radial ZnO electrode. Reproduced with permission.[51] Copyright 2014, Springer.

high reversibility of the electrode (Fig. 4f). Benefiting from the hollow radial architecture providing enormous void spaces and plenty of active sites, the electrodes revealed good cycling performance and rate capability for reversible lithium storage. For instance, the electrode held a reversible capacity of about 320 mA h g^{-1} at a current density of 0.2 A g^{-1} after 100 cycles.

The relationship between lithium ion storage performance and structural dimensions of ZnO-based anodes is systematically exhibited, suggesting the significance of structural design. The 0D ZnO nanostructures have exhibited potential to overcome the challenges existing in the traditional bulk materials owing to their unique nanostructural properties, presenting improved battery performance. ZnO electrodes with high-dimensional nanostructures commonly display better electron transmission rate, larger surface area, more interspaces to alleviate volume change, and more abundant ion diffusion pathways, promoting the reaction kinetics to some extent. Nevertheless, a series of issues accompany high-dimensional ZnO nanostructures, such as low initial coulombic efficiency resulting from extra lithium ion consumption for solid electrolyte interface (SEI) formation, and low packing density because of large numbers of voids within the nanostructures. Hence, rational structure design with different dimensions is necessary to develop high-performance ZnO electrodes.

4.2 Hybridization with carbonaceous materials

Other than structure design, introducing carbonaceous materials (graphene, carbon nanotubes, and derived carbon) has been demonstrated to be a promising way to overcome the inherent poor conductivity of the ZnO material.[25,54–64] Additionally, these carbon materials with good mechanical ductility can act as a buffer matrix to relieve the huge volume expansion during the charging/discharging process.

4.2.1 Graphene. Graphene, a 2D carbon layer of sp^2-bonded carbon atoms arranged in a hexagonal crystal lattice with one-atom thickness, has attracted much attention for various applications.[65] Graphene possesses fascinating properties, such as excellent electrical conductivity, high specific surface area (>2500 m^2 g^{-1}), superior mechanical strength, and good thermal/chemical stability. Therefore, a great number of researchers have focused on designing various ZnO/graphene composites for high-performance LIBs.[66–73]

Hsieh *et al.* reported that highly-crystalline ZnO nanocrystals with a size of 80–100 nm were uniformly anchored on both sides of graphene nanosheets (GN) by an efficient method (Fig. 5a).[74] The ZnO/GN composites with an optimum ratio showed a superior cycling stability with only 8% capacity decay after 50 cycles (Fig. 5b). Moreover, an excellent rate performance was also achieved, with 60% capacity retention, even with the current density increasing from 0.07 A g^{-1} to 3.5 A g^{-1}. These excellent electrochemical properties were attributed to rational structure design and composition regulation. The ZnO nanocrystals could efficiently prevent the restacking of graphene nanosheets. Meanwhile, the graphene nanosheets not only provided a high conductive network, but also exhibited a wide buffering effect to accommodate the volume change.

Sun and co-workers prepared uniform ZnO quantum dots (QDs) with size ranging from 2 to 7 nm homogeneously anchored along wrinkled graphene sheets by an atomic layer deposition (ALD) method (Fig. 5c).[75] According to the investigation of the relationship between the size and the electrochemical performance, they found that smaller-sized QDs on graphene exhibit better electrochemical performance. For 2 nm ZnO QDs, a high reversible specific capacity of 960 mA h g^{-1} was achieved by deducting the graphene contribution from the composites, approaching the theoretical specific capacity. Moreover, the comparison of
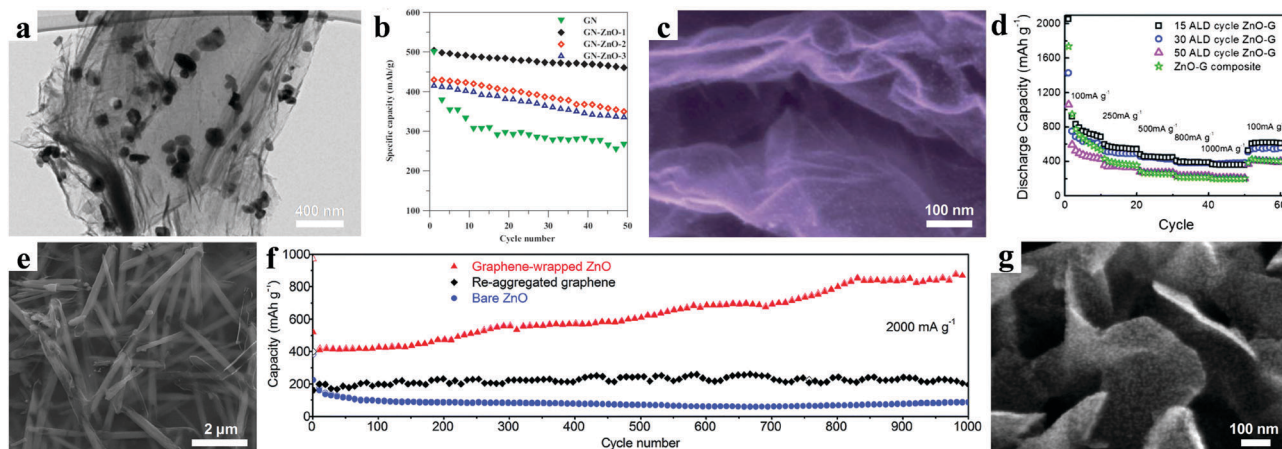
This journal is © The Royal Society of Chemistry and the Chinese Chemical Society 2018

Mater. Chem. Front., 2018, **2**, 1414–1435 | **1419**

Fig. 5 (a) TEM image of ZnO@GN composite; (b) cycling performances at 1C. Reproduced with permission.[74] Copyright 2013, Elsevier. (c) SEM image and (d) rate performances of graphene nanosheets coated by ZnO QDs. Reproduced with permission.[75] Copyright 2014, Royal Society of Chemistry. (e) SEM image of graphene-wrapped ZnO nanotubes; (f) cycling performance at 2 A g^{-1}. Reproduced with permission.[76] Copyright 2016, Royal Society of Chemistry. (g) SEM image of ZnO-VAGNs. Reproduced with permission.[77] Copyright 2014, American Chemical Society.

the rate performances showed that the appropriate proportion of ZnO and graphene is critical to obtaining high rate capability (Fig. 5d). A graphene-wrapped ZnO nanotube structure was synthesized by using graphene oxide nanosheets as a "soft" sealing layer confining the growth of ZnO nanotubes, as shown in Fig. 5e.[76] An impressive cycling stability with a high reversible specific capacity of 891 mA h g^{-1} over 1000 cycles at a current of 2 A g^{-1} was achieved (Fig. 5f).

In order to avoid the use of insulating binder, Li *et al.* prepared vertically aligned graphene nanosheets (VAGNs) grown *in situ* on Cu foil.[77] Then ultra-small ZnO nanoparticles uniformly grew on both sides of the VAGNs as a result of a hydrothermal process (Fig. 5g). Owing to the improved electrical conductivity and reduced Li ion transport path, the ZnO-VAGNs composites revealed excellent electrochemical performance. After 100 cycles, the reversible capacity still remained at 809 mA h g^{-1} at a charging/discharging current of 0.08 A g^{-1}, displaying good capacity retention.

4.2.2   Carbon nanotubes (CNTs). CNTs possess a series of fascinating properties, such as extraordinary conductivity (104 S cm^{-1}), high specific surface area, and excellent thermal and mechanical properties, which are considerably beneficial for energy storage applications. It is worthy of note that new possibilities in promoting the electrochemical properties have been created by constructing ZnO/CNTs composites.[78–83]

CNTs-supported ZnO composites were synthesized *via* an *in situ* co-precipitation process, in which ZnO nanohexagonal disks were well dispersed on the surface of the modified CNTs (Fig. 6a).[79] As displayed in Fig. 6b, the ZnO/CNT electrodes showed a reversible capacity of 602 mA h g^{-1} after 50 cycles, which was much higher than that of the bare ZnO electrodes (478 mA h g^{-1}). Köse *et al.* reported free-standing ZnO and multi-walled carbon nanotube (MWCNT) nanocomposites prepared with two different chelating agent additives, namely, triethanol-amine (TEA) and glycerin (GLY) (Fig. 6c).[81] It is interesting that the chelating agent additives have an effect on the

electrochemical performance of ZnO/MWCNT nanocomposites. With regard to the rate capability, as shown in Fig. 6d, the ZnO/MWCNT/GLY free-standing anode reached a capacity of 375 mA h g^{-1} at 2C, which is obvious higher than that of ZnO/MWCNT/TEA. In addition, the ZnO/MWCNT/GLY anode also delivered a higher discharge capacity – as high as 460 mA h g^{-1} – than the capacity of 180 mA h g^{-1} for the ZnO/MWCNT/TEA anode after 100 cycles at 0.2C. The authors suggested that the better performance of ZnO/MWCNT/GLY composites resulted from their smaller ZnO crystallite size, thinner ZnO film and mesoporous morphology.

4.2.3   Metal organic frameworks (MOFs)-derived carbon. MOFs, as an emerging class of crystalline inorganic–organic hybrid materials, possess uniform pore size and large specific surface area as well as diverse coordination structures, and are considered a promising template/precursor from which to prepare porous carbons. In addition, MOF structures have also been used to develop well dispersed ultrathin metal oxide nanoparticles embedded in porous carbon matrices. Here the MOFs-derived porous carbon skeleton demonstrates multiple functions, including enhancing the electrical conductivity, relieving the volume expansion, and avoiding the agglomera-tion of metal oxide nanoparticles. Recently, various Zn-based MOF precursors or sacrificial templates have been used to construct ZnO-based nanoarchitectures for LIBs.[26,84–92]

Yang *et al.* converted the metal–organic framework IRMOF-1 into porous carbon-coated ZnO QDs ($\sim$3.5 nm) *via* pyrolysis at high temperature.[93] Fig. 7a and b confirm that the highly crystalline ZnO QDs were well dispersed without agglomeration in the amorphous carbon matrix. When evaluated as an anode for lithium ion batteries, the porous carbon-coated ZnO QDs electrode exhibited a remarkable cycling stability with nearly 100% capacity retention after 50 cycles and an outstanding rate performance of 400 mA h g^{-1} at 3.75 A g^{-1}. In another representative work, Han *et al.* proposed a strategy by coating ZIF-8 nanoparticles with chitosan, and then the coated ZIF-8
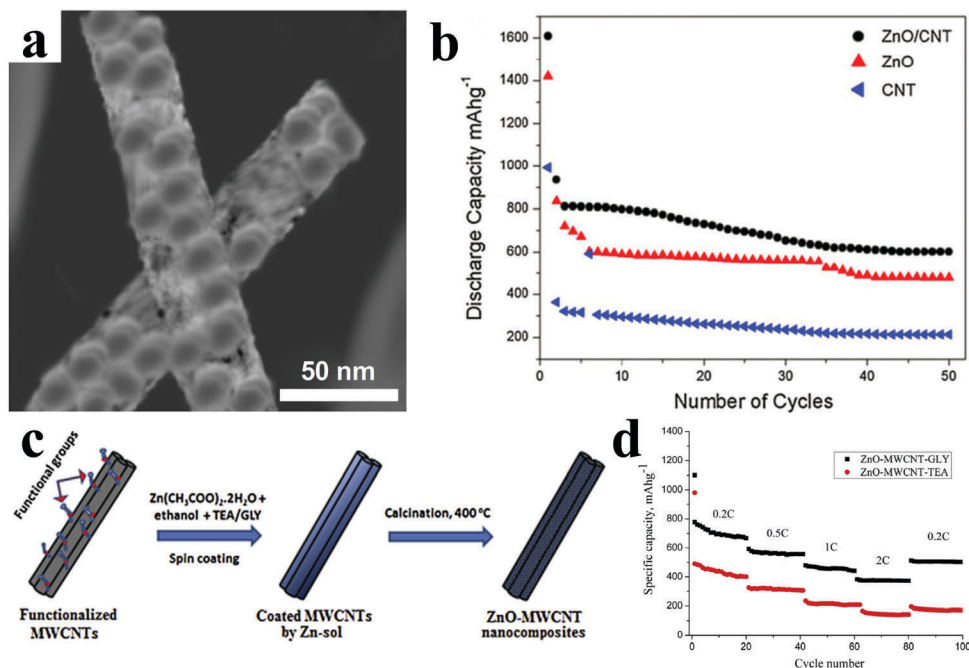
Fig. 6   (a) TEM image of ZnO/CNT composites; (b) cycling performances of bare CNTs, ZnO, and ZnO/CNT electrodes. Reproduced with permission.[79] Copyright 2013, Springer. (c) Schematic illustration of facile sol–gel synthesis of nanocomposite anodes; (d) the rate capabilities of the ZnO/MWCNT buckypaper nanocomposite anodes. Reproduced with permission.[81] Copyright 2015, Elsevier.
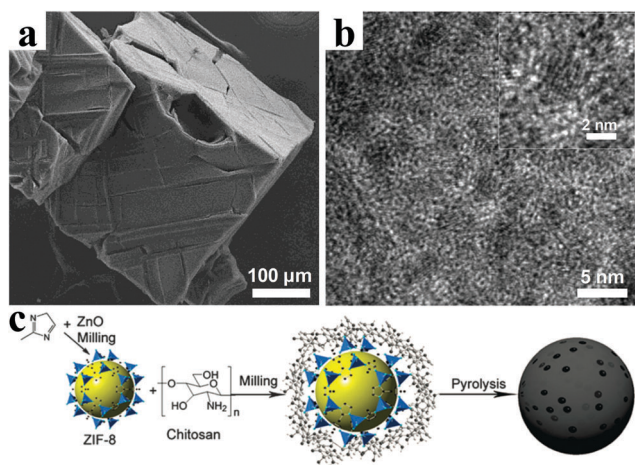

Fig. 7   (a) SEM image and (b) TEM image of ZnO QDs@porous carbon. Reproduced with permission.[93] Copyright 2013, American Chemical Society. (c) Synthetic route of ZIF-8@chitosan–800N. Reproduced with permission.[94] Copyright 2014, Royal Society of Chemistry.

was further pyrolyzed at 800 °C (Fig. 7c).[94] This strategy can effectively enhance the electrochemical performance of LIBs. As a result, a reversible capacity of 750 mA h g^{-1} was obtained at a current density of 0.05 A g^{-1}, and 99.6% capacity was retained after 50 cycles.

It is worth noting that our group constructed self-supported ZnO@ZnO QDs/C core–shell nanorod arrays (NRAs) via an ionic exchange route (Fig. 8a).[95] Ultimately, an integrated, binder-free, and lightweight ZnO@ZnO QDs/C electrode was obtained, as shown in Fig. 8b. As clearly displayed in Fig. 8c, the ZnO QDs

were wrapped by ZIF-8-derived porous carbon matrices with a thickness of several nanometers. The carbon matrices protected both the ZnO particles and the residual ZnO core from aggregating and expanding. Meanwhile, abundant meso-pores were beneficial for lithium ion access and transport, which could result in high cycling performance and excellent rate capability. When directly used as the anode, the ZnO@ZnO QDs/C core–shell NRAs presented a high first-cycle coulombic efficiency of around 92% and an outstanding rate capability (Fig. 8d and e). It was concluded that the integration of ZnO@ZnO QDs/C and current collector without using binder reduced interface resistance, ensuring fast electron transport; furthermore, the in situ coating of the MOF-derived N-doped porous carbon suppressed the volume expansion of ZnO, guaranteeing superior cycling stability. Similarly, Li et al. provided new insight into the preparation of nanomaterials via the pyrolysis of MOFs.[96] ZnO nanosheets grown on MOF-derived porous carbon matrix were synthesized by controlling the intermediate structures of MOF precursors during the pyrolysis process by introducing terephthalic acid and triethylenediamine as ligands (Fig. 8f). These ZnO nanosheets had an average thickness of 18.2 nm based on statistical results. The cycling performance of the composites manifested a rather high specific capacity of 920 mA h g^{-1} after 150 cycles at a current density of 0.05 A g^{-1}, suggesting a promising prospect in lithium storage application.

4.2.4 Other derived carbon. Importantly, other carbon materials, derived from various precursors such as organic polymers, organic acids and organometallic complexes, also enormously extend the application of carbon-coated
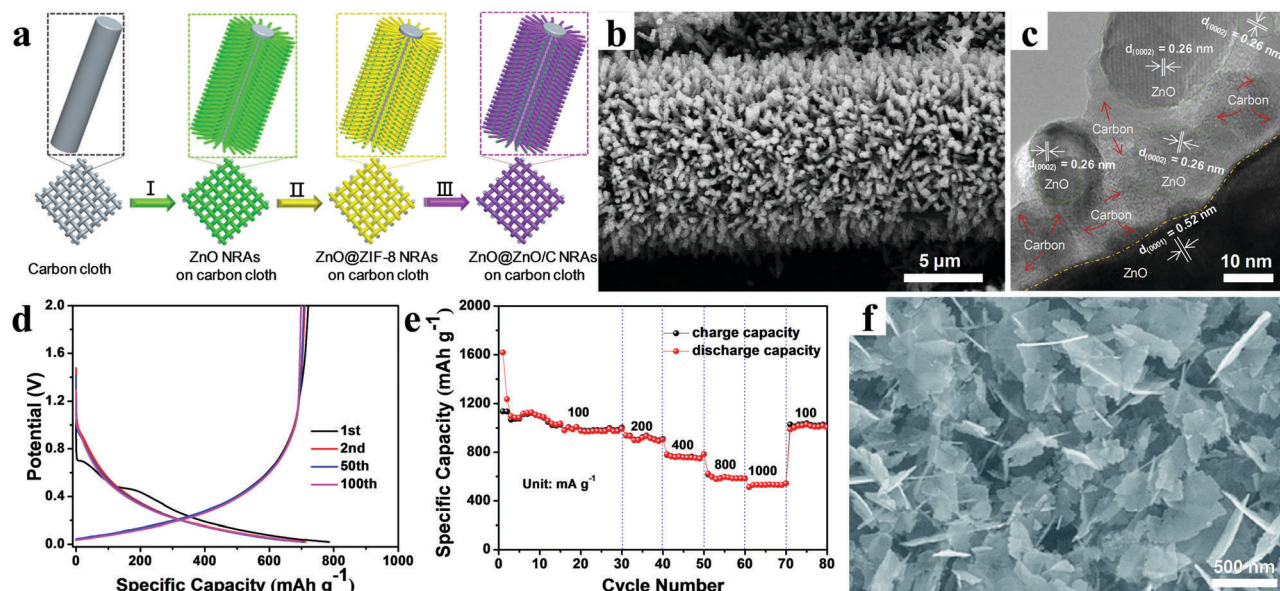
Fig. 8 (a) Schematic illustrating the synthesis procedure, (b) SEM image, (c) TEM image, (d) galvanostatic charging/discharging profiles, and (e) rate performance of core–shell ZnO@ZnO QDs/C NRAs grown on flexible carbon cloth. Reproduced with permission.[95] Copyright 2015, Wiley-VCH. (f) SEM image of ZnO nanosheets grown on porous carbon matrix. Reproduced with permission.[96] Copyright 2017, Royal Society of Chemistry.

ZnO composites.[97–111] The electrochemical performance of ZnO-based electrodes could be greatly improved by introducing these carbon materials; a great number of investigations have demonstrated that the carbon sources and the synthesis method have a significant effect on the ultimate promotion level. Thus, future work will focus on seeking suitable carbon precursors and developing a facile and large-scale synthetic method to produce the best electrochemical properties.

Recently, we proposed a solid-solution-like (SSL) concept to prepare ZnO/C composite nanofibers as anode materials for LIBs by a simple electrospinning technology, using polyacrylo-nitrile (PAN) as carbon source (Fig. 9a).[98] In this SSL nano-structure, amorphous ZnO was atomically "dissolved" in a carbon matrix to maximize the synergistic effect by creating the most metal oxide/carbon interfaces and defects possible, as shown in Fig. 9b. The composite nanofibers showed a high reversible capacity of 813.3 mA h g^{-1} after 100 cycles at a
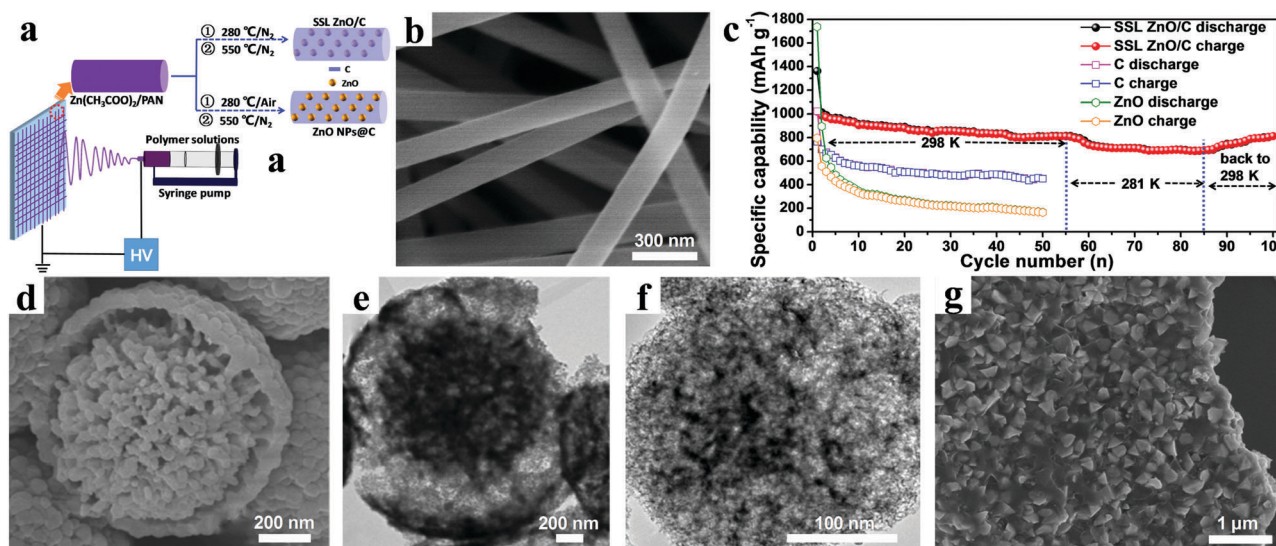
Fig. 9 (a) Schematic illustration of preparation process of SSL ZnO/C and ZnO NPs@C composites; (b) SEM image of SSL ZnO/C NFs; (c) cycling performance of SSL ZnO/C NFs at 0.1 A g^{-1} under the various ambient temperatures. Reproduced with permission.[98] Copyright 2015, Elsevier. (d) SEM image and (e) TEM image of yolk–shell structured YC–ZnO. Reproduced with permission.[100] Copyright 2017, Elsevier. (f) TEM image of a single ZnO–NMPCS particle. Reproduced with permission.[103] Copyright 2016, Elsevier. (g) SEM image of ZnO@C-5. Reproduced with permission.[105] Copyright 2014, Elsevier.

current density of 0.1 A g^{-1} (Fig. 9c). Furthermore, an outstanding rate performance was also demonstrated: even when the current density was increased by 40 times, the discharge capacity still remained at 53.5% of the initial value. Fan *et al.* used polyvinyl pyrrolidone (PVP) as the carbon source to synthesize hierarchical yolk–shell carbon-coated ZnO microspheres (YC-ZnO), as shown in Fig. 9d and e.[100] An impressive performance delivering a discharge capacity of 659 mA h g^{-1} was retained after 300 cycles at a current density of 0.5 A g^{-1}. Even with high current density of up to 10 A g^{-1}, the YC-ZnO electrodes also manifested superior cycling stability, with 96.9% capacity retention after 5000 cycles.

Sun *et al.* prepared a mesoporous N-doping spherical carbon matrix from melamine and phenol precursors.[103] Then a novel ZnO/carbon mesoporous composite (ZnO–NMPCS) was formed by the confined growth of ZnO nanoparticles in the carbon sphere (Fig. 9f). As a result, the developed ZnO–NMPCS nanocomposite exhibited an excellent cycling stability, with a capacity of 1058.9 mA h g^{-1} after 100 cycles at a current density of 0.2 A g^{-1}. Moreover, a capacity of 425 mA h g^{-1} after 1800 cycles was obtained even at a current density of 5 A g^{-1}. A composite material consisting of tetrahedral ZnO nanocrystals embedded in a three-dimension (3D) carbon framework derived from oleic acid and oleylamine was designed and fabricated *via* a simple internal-reflux method by Ren and co-workers (Fig. 9g).[105] When treated by subsequent calcination at 500 °C, the ZnO@C composite demonstrated the best electrochemical performance. For instance, a high capacity of 518 mA h g^{-1} was achieved after 300 cycles under a current density of 0.11 A g^{-1}. Chae *et al.* synthesized nano-sized ZnO/C composites to investigate the role of carbon in the electrochemical properties, citric acid being chosen as carbon precursor.[107]

Compared with the pure ZnO electrodes, the ZnO/C composite electrodes showed obviously enhanced rate capability and cycling performance. After 200 cycles, the ZnO/C composite electrodes held a reversible capacity of 700 mA h g^{-1} at a current density of 0.1 A g^{-1}.

As a typical organometallic complex, $C_4H_4ZnO_6$, as the precursor for both ZnO and carbon, was pyrolyzed in an inert atmosphere to prepare zinc oxide nanoparticles embedded in a carbon framework (ZnO@C).[108] Benefiting from the *in situ* introduction of carbon, the ZnO@C composite displayed an initial reversible capacity of 680 mA h g^{-1} at 1 A g^{-1}, and 89.7% capacity retention even after 300 cycles.

4.3 Doping with metal/metal ion

Heteroatom doping is another important way to improve the electrochemical properties of electrode materials, which can obviously enhance the electrical conductivity. A variety of metal/metal ions, including Au, Ag, Co, Cu, Sn, Ni, Mn, Al, and Fe, have been doped into ZnO-based materials.[112–128] In general, for the metal doping, the heteroatoms and ZnO are hybridized at the nanoscale level. However, for metal ion doping, the doping occurs at the atomic level by substituting Zn in the lattice by other metals. Large numbers of results have certified that this modified strategy highlights a promising approach to develop high-performance ZnO-based electrode materials.

For instance, Peng and coworkers combined a facile electrostatic attraction approach and subsequent annealing treatment in argon to produce sandwich-like Ag–C@ZnO–C@Ag–C hybrid hollow microspheres (Fig. 10a and b).[129] As the anode materials for LIBs, the composites revealed a very high reversible capacity of 1670 mA h g^{-1} after 200 cycles at a current density of 0.2 A g^{-1} (Fig. 10c). Meanwhile, at current densities of 1.6 and 10 A g^{-1},
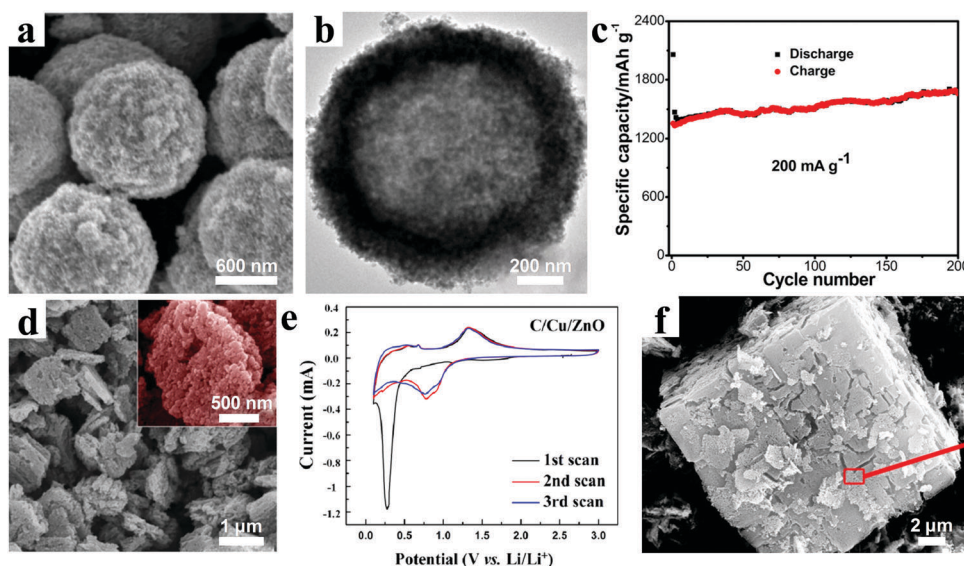
Fig. 10 (a) SEM and (b) TEM images of sandwich-like Ag–C@ZnO–C@Ag–C hybrid hollow microspheres; (c) cycling performances at 0.2 A g^{-1}. Reproduced with permission.[129] Copyright 2015, American Chemical Society. (d) SEM image and (e) CV curves of the C/Cu/ZnO hybrids. Reproduced with permission.[130] Copyright 2014, American Chemical Society. (f) SEM image of the CZO@C. Reproduced with permission.[131] Copyright 2014, American Chemical Society.

This journal is © The Royal Society of Chemistry and the Chinese Chemical Society 2018

Mater. Chem. Front., 2018, **2**, 1414–1435 | **1423**

specific capacities of about 1063 and 526 mA h g^{-1}, respectively, could be retained. These superior electrochemical performances resulted from the modification of silver and 3D carbon framework, as well as hollow nanostructure. As we know, Cu not only possesses high electrical conductivity, but also has a considerably lower cost than noble metals. C/Cu/ZnO porous hybrids were prepared by Wang and co-workers, in which the sizes of ZnO and Cu nanoparticles were distributed in the range 5–10 nm, as shown in Fig. 10d.[130] The current–voltage (C–V) curves after the first cycle are almost coincident, indicating excellent reversibility of the C/Cu/ZnO electrode (Fig. 10e). The cycling performance showed high and stable specific capacities of 818 mA h g^{-1} and 689 mA h g^{-1} at current densities of 0.05 A g^{-1} and 0.2 A g^{-1}, respectively, after 100 cycles. Yue et al. synthesized Co-doped MOF-5s by a secondary growth method, and then obtained Co-doped ZnO coated with carbon (CZO@C) by heat treatment under a nitrogen atmosphere (Fig. 10f).[131] Interestingly, they found that the doping with Co had a dual function, including improving the conductivity of the material and enhancing the graphitization degree of the carbon in the material, which was beneficial for fast electron transfer. Based on the synergetic effect of Co doping and carbon coating, the CZO@C showed a high reversible capacity of 725 mA h g^{-1} at a current density of 0.1 A g^{-1} after 50 cycles, which was much higher than that of ZnO@C composites without Co doping (335 mA h g^{-1}).

Bresser et al. presented n-type transition-metal (TM)-doped zinc oxide nanoparticles with the general formula $Zn_{0.9}TM_{0.1}O$ (TM = Fe or Co), in which the transition metals mixed with zinc on the atomic level rather than on the microscale or nanoscale, Zn atoms being replaced by transition metal atoms within the wurtzite lattice (Fig. 11a and b).[132] The results of in situ X-ray diffraction revealed that the alloying of lithium and zinc and the reduction of iron and zinc occurred simultaneously to a large extent. The Fe-doped ZnO nanoparticles displayed obviously enhanced specific capacities and rate performance compared with pristine zinc oxide when used as lithium ion anode. Inspired by natural fibrous roots, Yu et al. designed $Zn_xCo_{3-x}O_4@Zn_{1-y}Co_yO$ binary TMO nanoarrays on Cu substrates as an integrated LIB anode, in which the $Zn_{1-y}Co_yO$ nanowires acted as the root part and the $Zn_xCo_{3-x}O_4$ nanorods were the fibrous part (Fig. 11c).[133] Owing to the synergistic effect, the binary TMO nanoarray electrodes could hold a high reversible capacity of 804 mA h g^{-1} after 100 cycles at 0.5 A g^{-1}, which was much higher than that of the unitary cobalt-based and zinc-based nanoarrays.

4.4 Compositing with metal oxides

ZnO-based composites synthesized by addition of other metal oxides, such as CoO_x, CuO, NiO, Fe_2O_3, SnO_x, TiO_2, MnO_x, Al_2O_3, and $ZnFe_2O_4$, have also demonstrated unique characteristics for high-performance LIBs.[134–163] They have an obvious effect in relieving the volume expansion and improving the specific capacity, owing to the synergistic effect between the components.

Fang et al. prepared 2D porous hybrid bimetallic Co_3O_4/ZnO nanosheets via a facile thermal treatment, using the synergistic effects between the two components for outstanding electrochemical capability (Fig. 12a).[164] A series of materials with different Co : Zn molar ratios (1 : 0, 2 : 1, 1 : 1, 1 : 2, and 0 : 1)
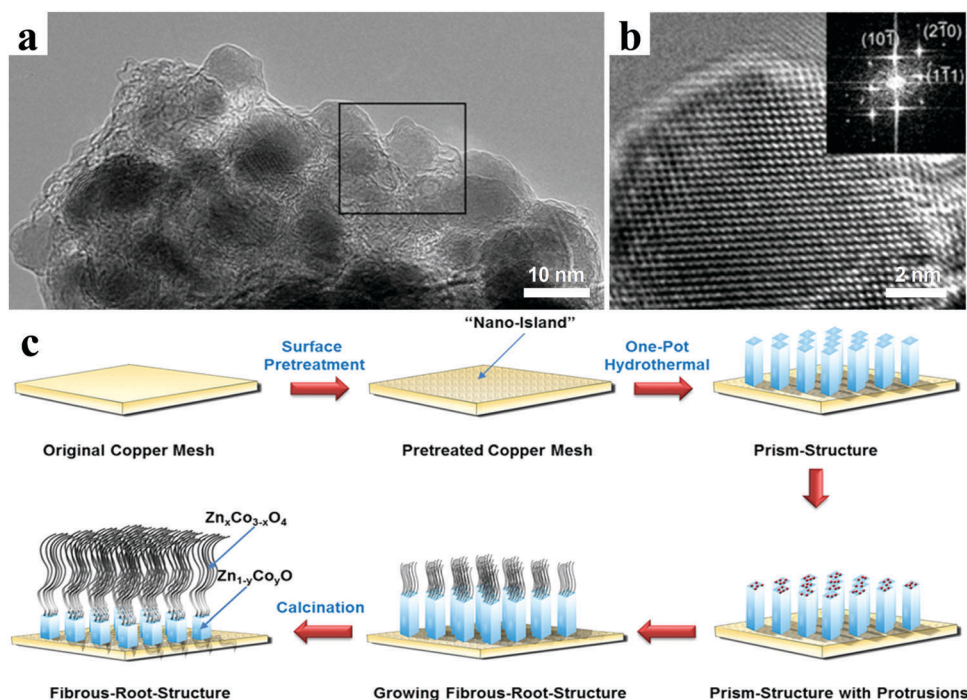
Fig. 11 (a) TEM and (b) HRTEM images of Fe-doped ZnO nanoparticles, inset in panel (b) showing the corresponding FT. Reproduced with permission.[132] Copyright 2013, American Chemical Society. (c) Preparation procedure of $Zn_xCo_{3-x}O_4@Zn_{1-y}Co_yO$ binary nanoarrays. Reproduced with permission.[133] Copyright 2016, American Chemical Society.

1424 | Mater. Chem. Front., 2018, 2, 1414–1435

This journal is © The Royal Society of Chemistry and the Chinese Chemical Society 2018

Fig. 12 (a) Schematic of the synthesis of 2D porous hybrid Co_3O_4/ZnO nanosheets. Reproduced with permission.[164] Copyright 2017, Royal Society of Chemistry. (b) TEM image of SnO_x–ZnO CNFs. Reproduced with permission.[165] Copyright 2016, American Chemical Society. (c) SEM image and (d) SAED pattern of ZnO–NiO–Co_3O_4 hybrid nanoflakes. Reproduced with 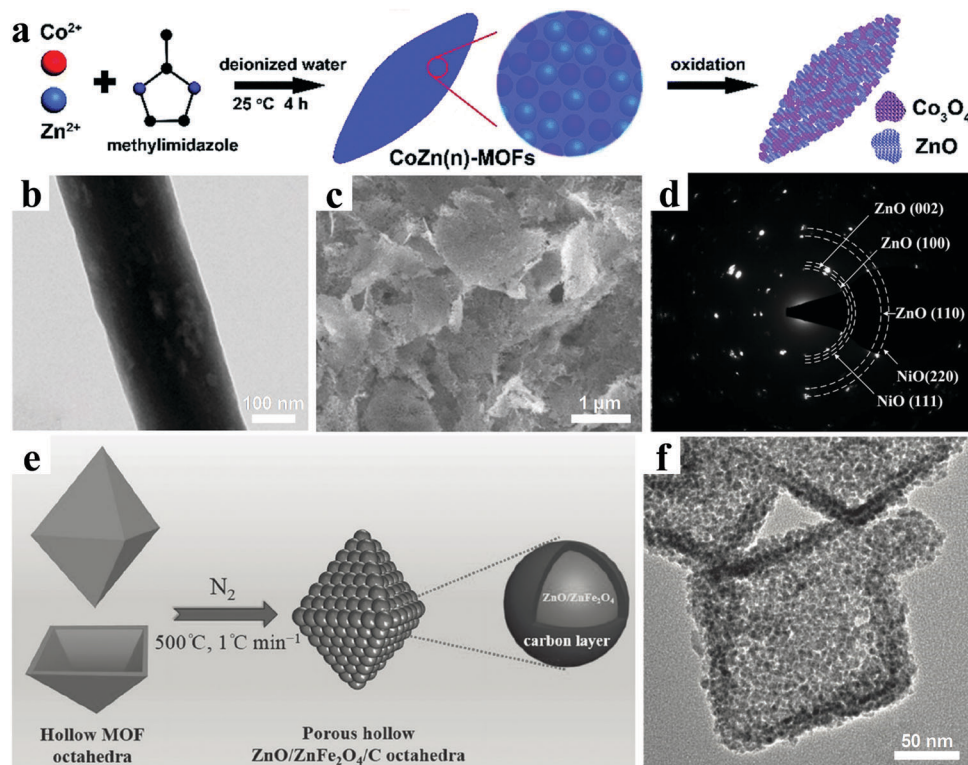permission.[166] Copyright 2017, Royal Society of Chemistry. (e) Schematic illustration for the preparation process and (f) TEM image of ZnO/$ZnFe_2O_4$/C nanoparticles. Reproduced with permission.[173] Copyright 2014, Wiley-VCH.

were designed and their corresponding electrochemical properties were compared in detail. The results suggested that the Co_3O_4/ZnO composite with the molar ratio of 1:1 showed the best electrochemical performance for LIBs, which benefited from an appropriate ratio of Co_3O_4 and ZnO and the electrochemical synergistic effects. Flexible, freestanding, and binder-free electrodes consisting of amorphous SnO_x–ZnO particles uniformly dispersed in carbon nanofibers (CNFs) were developed *via* a simple electrospinning method by Joshi *et al.* (Fig. 12b).[165] Compared with pure CNFs, ZnO CNFs, and SnO_x CNFs electrodes, SnO_x–ZnO CNFs with a Sn:Zn ratio of 3:1 displayed the highest first discharge and charge capacities (1910 and 1400 mA h g^{-1}, respectively) and a high reversible capacity of 963 mA h g^{-1} at a current density of 0.1 A g^{-1} after 55 cycles. Lu *et al.* developed ZnO–NiO–Co_3O_4 hybrid nanoflakes based on the idea of introducing a small amount of Co_3O_4 as a catalyzing and performance-enhancing agent (Fig. 12c and d).[166] Although only a small amount was present, Co_3O_4 played a vital role as it can further enhance the conductivity and catalytic activity of the hybrid materials. When applied as anode materials, the hybrid nanoflakes exhibited an excellent reversible capacity of 1060 mA h g^{-1} after 300 cycles at a current density of 0.5 A g^{-1}.

Recently, nanostructured ZnO and ternary ZnM_2O_4 (M = Ge, Fe, Co *etc.*) composites have generated increasing interest as promising lithium-storage materials for LIBs.[167–172]

Zou *et al.* reported porous hollow ZnO/$ZnFe_2O_4$/C octahedra using a MOF as both the precursor and the self-sacrificing template by an ordinary refluxing reaction followed by thermal annealing in N_2, as shown in Fig. 12e.[173] In the nanostructure, ultrafine ZnO and $ZnFe_2O_4$ nanocrystals of less than 5 nm were uniformly embedded in a 3D interconnected, porous carbon framework (Fig. 12f). An outstanding electrochemical lithium-storage performance was demonstrated, in which superior specific capacities were as high as 1390 mA h g^{-1} and 988 mA h g^{-1} after 100 cycles at the current densities of 0.5 A g^{-1} and 2 A g^{-1}, respectively. The rate performance exhibited a specific capacity of 762 mA h g^{-1} even at a high current density of 10 A g^{-1}.

An intriguing phenomenon, that nano-sized Zn-based composite anodes always deliver higher specific capacities than the theoretical capacity, has been reported in the literature.[68,76,77,113] Similar to other nano-sized transition-metal oxides, the extra capacity may originate from the formation of polymer/gel-like film, the surface/interface lithium ion storage and synergistic effects of composites.[93,123,126,133,174–177] For example, the hybrid ZnO QDs@porous carbon anode exhibited a reversible capacity of 1150 mA h g^{-1}, which was obviously beyond the theoretical capacity of 817 mA h g^{-1} considering the relative amounts of ZnO and amorphous carbon.[93] The extra capacity came from interfacial charge storage *via* weak bonding between Li^+ and the surface of ZnO QDs, reactions with the electrolyte, charge separation at the SEI layer, and synergistic effects of the

composites of ZnO and amorphous carbon. The mechanism of this phenomenon needs to be further studied in order to better optimize the performance of the Zn-based negative electrodes from the aspects of structure design and component control.

5. Other Zn-based nanomaterials

In addition to ZnO, lots of other Zn-based nanomaterials, such as ZnS, ZnSe, ZnP, ZnSb, and ZnTe, have also been reported as attractive anode candidates for Li ion batteries. Generally, these Zn-based nanomaterials show different advantages for electrochemical features owing to their different properties.

As a kind of typical transition metal sulfide, ZnS has been considered a promising electrode material for next-generation LIBs, owing to its high theoretical specific capacity of 962.3 mA h g^{-1}. Unfortunately, similar to ZnO electrodes, the huge volume and structure changes in the lithiation/delithiation process and the poor conductivity greatly hinder the practical application of ZnS-based electrodes. Rational structure design, by reducing the size to the nanoscale and hybridizing with conductive carbonaceous materials, has been demonstrated an effective strategy for improving the lithium storage performance. Up to now, various carbonaceous materials, such as citric acid, graphene, porous carbon, reduced graphene oxide, C_2H_2, and glucose, have been adopted to alleviate the volume variations and enhance the electrical conductivity of ZnS electrodes, which has usually resulted in obviously improved electrochemical performances.[178–185] Especially, Li *et al.* prepared ZnS nanoparticles decorated on nitrogen-doped porous carbon (NPC) polyhedra by carbonizing

and vulcanizing zeolitic imidazolate framework-8 (ZIF-8) with polyhedral morphology (Fig. 13a and b).[186] Thus a ZnS/NPC hybrid showed a high reversible specific capacity of 1067.4 mA h g^{-1} at a current density of 0.1 A g^{-1} after 200 cycles. As shown in Fig. 13c, it displayed an excellent rate capability with a specific capacity of 364.6 mA h g^{-1} even at 4 A g^{-1}. It exhibited superior long cycling performance, with a reversible capacity of 856.8 mA h g^{-1} after 1000 cycles at a high current density of 1 A g^{-1}.

As another kind of typical metal chalcogenide, ZnSe possesses a high theoretical capacity of 557 mA h g^{-1} based on the alloying and conversion reaction mechanism.[187] Thus, numerous efforts have been made to realize its much better performance as anode for LIBs.[188,189] In order to address the drawbacks of huge volume change up cycling and the intrinsic low electrical conductivity, composites of ZnSe and carbon are considered promising electrode materials with an obvious enhanced electrochemical performance.[190–192] Chen *et al.* designed three-dimensional composites consisting of ZnSe nanodots uniformly confined within an N-doped porous carbon network, showing a high reversible capacity of 1134 mA h g^{-1} after 500 cycles at a current density of 0.6 A g^{-1} and excellent rate capability of 474 mA h g^{-1} at a current density of 12.8 A g^{-1} (Fig. 13d and e).[191] In general, ZnSe electrodes displayed rising and additional reversible capacities beyond their theoretical capacities during cycling. Xu *et al.* investigated the origin of the additional capacities in ZnSe@C composites by employing *ex situ* X-ray photoelectron spectroscopy and controlling the electrochemical charging/discharging process.[192] Their results showed that the generated and activated Se made the major contribution to the extra rising capacity in this system during the electrochemical process.
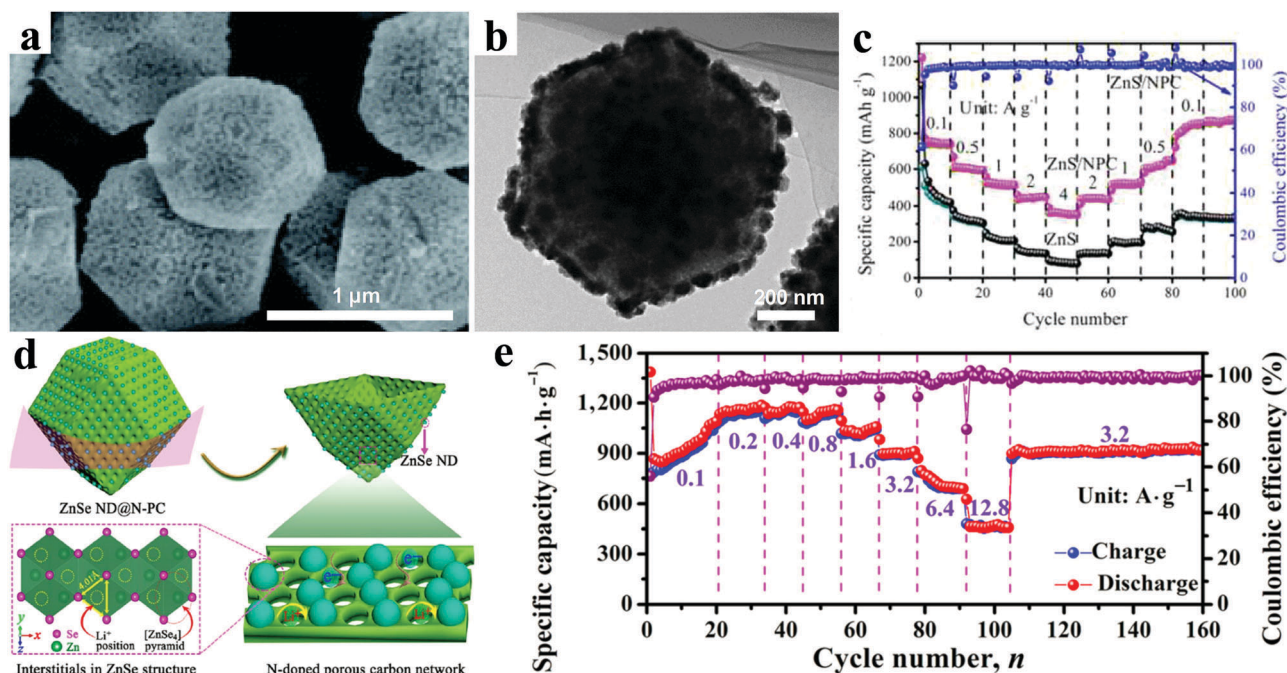
Fig. 13 (a) SEM image, and (b) TEM image of ZnS/NPC hybrid; (c) rate performances of ZnS/NPC and ZnS. Reproduced with permission.[186] Copyright 2017, Royal Society of Chemistry. (d) Schematic illustration for the construction of ZnSe ND@N-PC architecture; (e) rate capability at various current densities of ZnSe ND@N-PC composite electrodes. Reproduced with permission.[191] Copyright 2017, Tsinghua University Press and Springer.

1426 | *Mater. Chem. Front.*, 2018, **2**, 1414–1435

This journal is © The Royal Society of Chemistry and the Chinese Chemical Society 2018

As promising anode materials for LIBs, Zn_xP_2 (x = 1, 3) have also been reported by many research groups.[193,194] Bichat et al. obtained Zn_3P_2 powders with various morphologies by three different solid state preparation routes and revealed the Li insertion mechanism into the Zn_3P_2 electrode.[195] The Li ion storage process included two distinct but parallel reversible pathways: one pathway employed exclusively phosphide phases (Zn_3P_2, $LiZnP$, Li_4ZnP_2, and Li_3P) and the other pathway involved only Li–Zn alloys (Zn, $LiZn_4$, and LiZn). Self-supported Zn_3P_2 nanowire arrays grafted on different conductive substrates have been designed and directly used for electrodes.[196,197] For instance, Zn_3P_2 nanowire arrays on carbon fabric cloth as an integrated binder-free anode via a facile chemical vapor deposition (CVD) were reported by Li et al. (Fig. 14a).[197] The results showed an impressive electrochemical performance with a coulombic efficiency up to 88%, excellent cycling stability without obvious decay after 200 cycles, and high rate capability of 400 mA h g^{-1} even at 15 A g^{-1}. Compared with zinc-rich Zn_3P_2 (1241 mA h g^{-1}), phosphorus-rich ZnP_2 possesses a higher theoretical specific capacity (1581 mA h g^{-1}). Monoclinic ZnP_2, tetragonal ZnP_2, and orthorhombic ZnP_2 electrodes have been investigated. Recently, Chen et al. synthesized orthorhombic ZnP_2 nanowires with diameters ranging from 10 to 50 nm by a solvothermal method (Fig. 14b).[198] The electrochemical measurement results showed a high first discharge specific capacity of 1415 mA h g^{-1} at 0.3C with a high initial coulombic efficiency of 89% and an excellent cycling performance, which demonstrated that ZnP_2 nanowires are a promising anode material for lithium ion batteries.

Intermetallic compounds Zn_xSb_y, such as ZnSb and Zn_4Sb_3, have been investigated as anodes for LIBs.[199–202] Orthorhombic ZnSb possesses a puckered layer structure, in which Zn and Sb atoms are connected by screw-type layered chains along the b-axis. Park & Sohn reported the quasi-intercalation behavior of ZnSb reacting with Li ions.[203] During the charging process, the insertion of Li ions transformed the puckered hexagonal channels into regular hexagonal channels. Then, the layered Zn–Sb planes were rearranged, periodic Li arrays passed through the cleavage, and puckered Zn–Sb chains were recombined. The electrochemical testing results showed an excellent cycling stability with the ZnSb electrode demonstrating 80% capacity retention compared with the first discharge capacity after 1000 cycles at 0.1 A g^{-1}. Xu et al. directly grew one-dimensional Zn_4Sb_3 structures such as nanotubes, nanowires and nanorods on Cu foil by a simple CVD method (Fig. 14c).[204] The obtained Zn_4Sb_3 nanotubes exhibited better electrochemical performance than the other Zn_4Sb_3 structures, because the one-dimensional transport nature and the tubular structures are beneficial for high rate performance and excellent cycling durability. In Fig. 14d, a reversible capacity of 450 mA h g^{-1} after 100 cycles at a current of 0.1 A g^{-1} is demonstrated.

Recently, ZnTe has been proposed as a potential electrode material for rechargeable LIBs. ZnTe possesses a much higher density of 6.34 g cm^{-3} compared with those of ZnO (5.61 g cm^{-3}), ZnS (4.09 g cm^{-3}), and ZnSe (5.27 g cm^{-3}), which will result in high volumetric capacity when it is applied in the Li ion battery. Seo & Park prepared a ZnTe/C nanocomposite, composed of 5–10 nm ZnTe nanocrystallites uniformly distributed within a carbon matrix (Fig. 14e and f).[205] They revealed the reaction process during the first charging/discharging cycle was as follows:

$$ZnTe \rightarrow Li_2Te + Zn \rightarrow Li_2Te + Li_xZn$$
$$\rightarrow Li_2Te + LiZn \text{ (discharge process)} \quad (4)$$
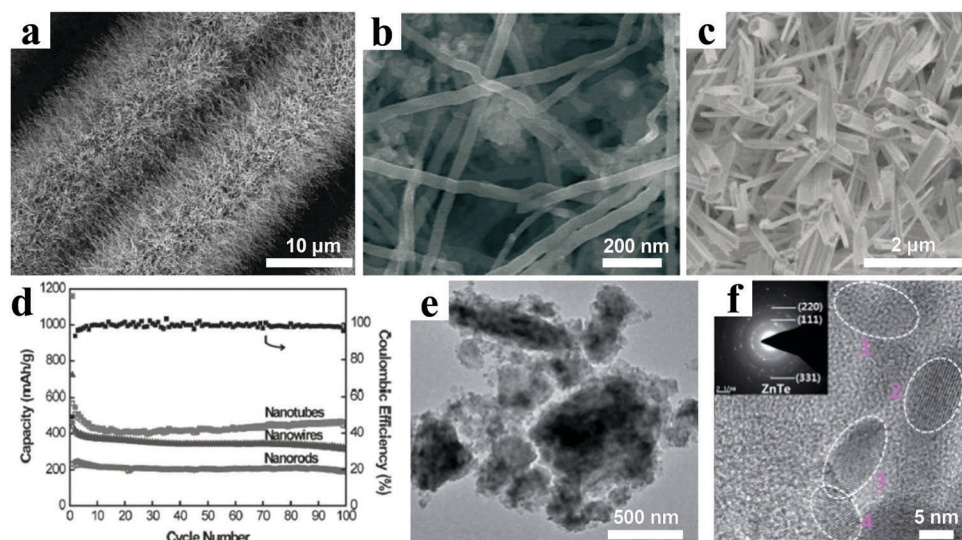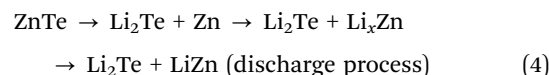
Fig. 14 (a) SEM image of Zn_3P_2 nanowire arrays grown on carbon cloth. Reproduced with permission.[197] Copyright 2016, Royal Society of Chemistry. (b) SEM image of ZnP_2 nanowires. Reproduced with permission.[198] Copyright 2017, Royal Society of Chemistry. (c) SEM image of Zn_4Sb_3 nanotubes deposited on copper foil; (d) cycling performances of Zn_4Sb_3 nanotubes, nanowires, and nanorods at 0.1 A g^{-1}. Reproduced with permission.[204] Copyright 2013, Wiley-VCH. (e) TEM image and (f) HRTEM image of ZnTe/C nanocomposite, insert showing the SAED pattern. Reproduced with permission.[205] Copyright 2014, Royal Society of Chemistry.

This journal is © The Royal Society of Chemistry and the Chinese Chemical Society 2018

Mater. Chem. Front., 2018, **2**, 1414–1435 | **1427**

$$Li_2Te + LiZn \rightarrow Li_2Te + Li_xZn \rightarrow Li_2Te + Zn$$
$$\rightarrow ZnTe \; (charge \; process) \qquad (5)$$
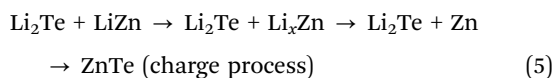
When applied as anode, the ZnTe/C nanocomposite showed an outstanding electrochemical performance: an initial charge capacity of 530 mA h g^{-1}, long cycling stability holding a specific capacity of 623 mA h g^{-1} over 200 cycles, and fast rate capability with 92% and 84% retention of the initial charge capacity at rates of 1C and 3C, respectively.

The above novel Zn-based nanomaterials demonstrate superior electrochemical performance including high specific capacity, excellent rate capability, and long cycling life. Compared with ZnO-based materials, these Zn-based electrodes exhibit a series of advantages, such as improved conductivity for ZnS, higher theoretical specific capacity for ZnP$_2$, and higher density for ZnTe. However, continuous efforts are still required to overcome challenges to the practical application of the novel Zn-based electrodes, such as low yields, high cost, complicated procedures, poor conductivity and structural stability.

In general, an SEI film will be formed during the first cycle, which results from the interface reaction of the active materials and the electrolyte. Owing to the irreversibility of Li$^+$ consumption in forming the SEI film, electrodes suffer a relatively large irreversible capacity loss, leading to a low initial coulombic efficiency. But the stable SEI film is favorable to avoid the further reaction of the active materials and the electrolyte and improve the electrochemical performance. During the charging/discharging process, traditional bulk Zn-based anodes undergo huge volumetric change and structural breaking, causing the continuous forming of the SEI film and low coulombic efficiency. Furthermore, the thus continuously thickened SEI film also reduces electrical contact between the active materials and the current collector. Nanostructural Zn-based anodes can effectively overcome the pulverization of electrode materials and form a stable SEI film. Unfortunately, larger irreversible capacity loss and lower initial coulombic efficiency are observed for nanostructural Zn-based anodes, because the high surface area of nanostructural materials provides more contact area between the electrodes and the electrolyte for interface reaction. Therefore, the irreversible capacity loss and the initial coulombic efficiency hold a close relationship with the size, structure and morphology of Zn-based materials.

Enormous efforts have been taken to ameliorate the initial coulombic efficiency of Zn-based anodes. Electrolyte optimization is another effective strategy to improve the lithium storage performance of Zn-based anodes through modifying the surface chemistry.[206–208] For example, the addition of fluoroethylene carbonate (FEC) in the electrolyte could promote the formation of a more uniform and stable SEI film and improve the electrochemical performance of the ZnCo$_2$O$_4$ electrode.[208] Additionally, coating a protective layer on the Zn-based materials, supplying additional Li resources for pre-lithiation, and modifying binder also have been deployed to reduce the irreversible capacity loss and improve the initial coulombic efficiency.[67,209–212]

6. Lithium ion full cells with Zn-based anodes

It is worth noting that the aforementioned progress of Zn-based anodes is based on half cells (Table 2). However, in order to further evaluate the performance and practical applicability of Zn-based composites, the study of Zn-based anodes assembled in full cells is desperately needed.[213] Zn-based anode full cells formed by coupling with commercial cathode materials (such as LiCoO$_2$, LiFePO$_4$, and LiNi$_{1/3}$Co$_{1/3}$Mn$_{1/3}$O$_2$) have been investigated by a few research groups (Table 3).[214–223]

Liu *et al.* directly grew 3D ZnCo$_2$O$_4$ nanowire arrays on flexible carbon cloth as a binder-free anode and coupled this anode with a conventional LiCoO$_2$ cathode to construct a flexible full cell (Fig. 15a).[215] The initial discharge capacity of 1314 mA h g^{-1} and the capacity retention of approximately 1300 mA h g^{-1} indicated a high reversibility (Fig. 15b). They also synthesized ZnCo$_2$O$_4$ urchins on carbon fiber cloth to fabricate high-performance flexible cells.[216] A full cell combining the ZnCo$_2$O$_4$ anode and a commercial LiCoO$_2$ cathode demonstrated a lithium storage capacity of 1172 mA h g^{-1} even after 50 cycles at 0.2C. Xiong *et al.* reported flexible full cells with 2D ZnMn$_2$O$_4$/graphene nanosheet anodes and LiFePO$_4$ nanosheet cathodes, considering the advantages of the unique 2D nanosheets, such as excellent electronic conductivity, short Li ion diffusion path, and more active surfaces (Fig. 15c).[218] The as-prepared full cells exhibited superior cycling performance and rate capability. Furthermore, the stable cycling behavior could still be obtained under bending, folding and rolling (Fig. 15d). An impressive cycling performance with 85% capacity retention after 10000 cycles based on carbon-coated ZnFe$_2$O$_4$ anode and LiFePO$_4$–CNT composite cathode coupled full cells was demonstrated by Varzi *et al.* (Fig. 15e).[220] In addition, the authors claimed that the observed maximum specific energy and power densities were 202 W h kg^{-1} and 3.72 kW kg^{-1}, respectively (Fig. 15f). However, the related research on Zn-based full cells is still limited, and more efforts should be made in this field.

7. Summary and outlook

In this review, we have summarized the most recent progress of zinc-based nanomaterials as LIB anodes. So far, the main modification methods used to improve the capability for lithium ion storage of ZnO-based anodes fall into four categories. First, various ZnO nanostructures with tunable dimensions have been rationally designed. Benefiting from rationally designed structures with more active sites and superior mechanical stability, these ZnO electrodes display obviously enhanced electrochemical performance. Second, combining ZnO with carbonaceous materials can not only effectively improve electronic conductivity of the electrodes, but also relieve the huge

Table 2 A summary of Zn-based anodes for lithium-ion half cells

Material	Synthesis method	1st discharge–charge capacity (mA h g^{-1})	Cycling stability	Rate capability (mA h g^{-1})	Ref.
ZnO nanoparticles	Ball milling	1100/683 at 0.1 A g^{-1}	570 mA h g^{-1} (200 cycles)	371 at 2C	33
ZnO nanosheets	Solvothermal	1523/$\sim$780 at 0.2 A g^{-1}	421 mA h g^{-1} (100 cycles)	325 at 1 A g^{-1}	46
ZnO/carbon black	Atomic layer deposition	$\sim$1572/1081 at 0.1 A g^{-1}	769.5 mA h g^{-1} (500 cycles)	$\sim$1014 at 0.5 A g^{-1} $\sim$810 at 2 A g^{-1}	60
ZnO QD/carbon bubble	CVD & annealing	1914/1054 at 0.1 A g^{-1}	510 mA h g^{-1} (400 cycles) at 1 A g^{-1}	530 at 1 A g^{-1} 210 at 8 A g^{-1}	61
ZnO/graphene oxide	Precipitation	$\sim$1540/780 at 0.1 A g^{-1}	752.8 mA h g^{-1} (65 cycles)	404.4 at 1 A g^{-1} 259.7 at 2 A g^{-1}	68
Graphene-wrapped ZnO nanotubes	Hydrothermal & annealing	1511/1011 at 0.1 A g^{-1}	891 mA h g^{-1} (1000 cycles) at 2 A g^{-1}	514 at 0.5 A g^{-1} 389 at 2 A g^{-1}	76
ZnO/multiwalled CNT	Precipitation & annealing	1477/845 at 0.1 A g^{-1}	419.8 mA h g^{-1} (100 cycles) at 0.2 A g^{-1}	326.8 at 1 A g^{-1}	82
ZnO@ZnO QDs/C core–shell NRAs	Hydrothermal & annealing	$\sim$1610/1160 at 0.1 A g^{-1}	699 mA h g^{-1} (100 cycles) at 0.5 A g^{-1}	530 at 1 A g^{-1}	95
ZnO nanosheet/porous carbon	Hydrothermal & annealing	$\sim$1920/880 at 0.05 A g^{-1}	920 mA h g^{-1} (150 cycles)	363 at 1 A g^{-1} 50 at 10 A g^{-1}	96
ZnO/C nanofibers	Electrospinning & annealing	1750/1319 at 0.1 A g^{-1}	452 mA h g^{-1} (500 cycles) at 2 A g^{-1}	591 at 2 A g^{-1}	97
YC-ZnO	Precipitation & annealing	1501/1168 at 0.1 A g^{-1}	$\sim$254 mA h g^{-1} (5000 cycles) at 10 A g^{-1}	485.7 at 2 A g^{-1} 289.6 at 10 A g^{-1}	100
ZnO-NMPCS	Sol–gel & hydrothermal	2627/1667 at 0.2 A g^{-1}	425 mA h g^{-1} (1800 cycles) at 5 A g^{-1}	840 at 0.2 A g^{-1} 471 at 4 A g^{-1}	103
Ge-Doped ZnO	CVD	1496.5/1014 at 0.1 A g^{-1}	$\sim$690 mA h g^{-1} (100 cycles)	$\sim$515 at 0.4 A g^{-1} $\sim$430 at 0.8 A g^{-1}	112
Co-Doped ZnO	Sol–gel & annealing	1338.7/1134.7 at 0.1 A g^{-1}	412.5 mA h g^{-1} (1000 cycles) at 1 A g^{-1}	370.4 at 3 A g^{-1}	123
Cu-Doped ZnO/carbon	Precipitation & annealing	1472/876 at 0.2 A g^{-1}	769 mA h g^{-1} (500 cycles)	350 at 1 A g^{-1}	124
Ag-Doped ZnO/carbon	Sol–gel & annealing	2396/1569 at 0.1 A g^{-1}	1670 mA h g^{-1} (200 cycles) at 0.2 A g^{-1}	1063 at 1.6 A g^{-1} 526 at 10 A g^{-1}	129
Co-Doped ZnO	Hydrothermal & annealing	1692/1241 at 0.5 A g^{-1}	804 mA h g^{-1} (100 cycles)	738 at 1 A g^{-1}	133
ZnO/ZnFe$_2$O$_4$ submicrocubes	Precipitation & annealing	1892/1371 at 0.1 A g^{-1}	837 mA h g^{-1} (200 cycles) at 1 A g^{-1}	728 at 1 A g^{-1} 667 at 2 A g^{-1}	163
Co$_3$O$_4$/ZnO nanosheets	Precipitation & annealing	$\sim$690/420 at 0.1 A g^{-1}	442 mA h g^{-1} (1000 cycles) at 3 A g^{-1}	404 at 4 A g^{-1}	164
SnO$_x$/ZnO/C nanofibers	Electrospinning & annealing	1910/1400 at 0.1 A g^{-1}	963 mA h g^{-1} (55 cycles)	600 at 0.5 A g^{-1} 400 at 1 A g^{-1}	165
Co$_3$O$_4$/NiO/ZnO nanoflakes	Hydrothermal & annealing	1454/993 at 0.1 A g^{-1}	1060 mA h g^{-1} (300 cycles) at 0.5 A g^{-1}	667 at 2 A g^{-1}	166
ZnO/ZnFe$_2$O$_4$/C	Precipitation & annealing	1385/1047 at 0.5 A g^{-1}	1390 mA h g^{-1} (100 cycles)	762 at 10 A g^{-1}	173
ZnS/C nanoparticles	Hydrothermal & CVD	1157/694 at 0.1 A g^{-1}	506 mA h g^{-1} (600 cycles) at 0.5 A g^{-1}	363 at 5 A g^{-1}	184
ZnS/porous carbon	Precipitation & annealing	1445.3/839.3 at 0.1 A g^{-1}	1067.4 mA h g^{-1} (200 cycles)	364.6 at 4 A g^{-1}	186
ZnSe nanodots/porous carbon	Precipitation & annealing	871/494 at 0.6 A g^{-1}	1134 mA h g^{-1} (500 cycles)	696 at 6.4 A g^{-1} 474 at 12.8 A g^{-1}	191
ZnP$_2$ nanowires	Solvothermal	1575/1415 at 0.3C	1066 mA h g^{-1} (500 cycles)	309 at 4C	198
Zn$_4$Sb$_3$ nanotubes	CVD	1160/$\sim$590 at 0.1 A g^{-1}	450 mA h g^{-1} (100 cycles)		204
ZnTe/C	Ball milling	690/530 at 0.1 A g^{-1}	623 mA h g^{-1} (200 cycles)	550 at 1C 504 at 3C	205

Table 3 Recent work on Zn-based anodes for lithium-ion full cells

Anode material	Cathode material	Capacity (mA h g^{-1})	Cycling stability	Rate capability (mA h g^{-1})	Ref.
ZnO/C	LiNi$_{0.6}$Co$_{0.2}$Mn$_{0.2}$O$_2$	180 at 0.1C	126.1 mA h g^{-1} (30 cycles) at 1C		214
ZnCo$_2$O$_4$ nanowires	LiCoO$_2$	1314 at 0.2 A g^{-1}	1300 mA h g^{-1} (40 cycles)		215
ZnCo$_2$O$_4$ urchins	LiCoO$_2$	1175 at 0.2C	1172 mA h g^{-1} (50 cycles)	$\sim$810 at 5C	216
ZnCo$_2$O$_4$ spheres	LiNi$_{1/3}$Co$_{1/3}$Mn$_{1/3}$O$_2$	$\sim$70 at 0.2C	$\sim$70 mA h g^{-1} (10 cycles)		217
ZnMn$_2$O$_4$/graphene	LiFePO$_4$	132 at 0.2C	124 mA h g^{-1} (100 cycles)	122 at 0.5C 90 at 2C	218
ZnFe$_2$O$_4$/graphene	LiFePO$_4$	805 at 0.1 A g^{-1}	$\sim$440 mA h g^{-1} (10 cycles)		219
ZnFe$_2$O$_4$/C	LiFePO$_4$/CNT		41 mA h g^{-1} (10 000 cycles) at 3 mA cm^{-2}		220

volume expansion during the charging/discharging process. Third, doping ZnO with highly conductive metal heteroatoms is an effective method to enhance the electronic conductivity of ZnO-based anodes, resulting in improved electrochemical properties. Fourth, compositing ZnO with other metal oxides produces outstanding electrochemical performance with the
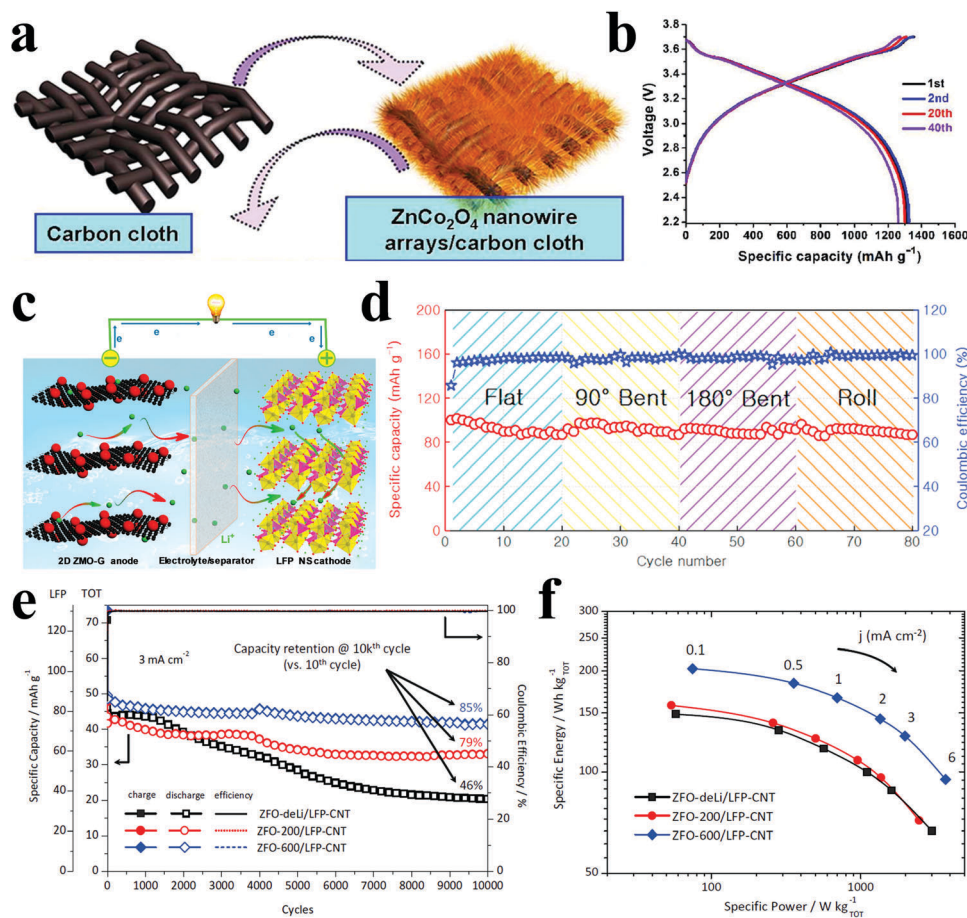
This journal is © The Royal Society of Chemistry and the Chinese Chemical Society 2018

Mater. Chem. Front., 2018, 2, 1414–1435 | 1429

Fig. 15 (a) Schematic illustration of the synthesis of flexible 3D $ZnCo_2O_4$ nanowire arrays/carbon cloth; (b) charging/discharging curves of the full flexible battery. Reproduced with permission.[215] Copyright 2012, American Chemical Society. (c) Schematic of Li-ion full cell using 2D $ZnMn_2O_4$/grapheme (ZMO−G) nanosheet anode and $LiFePO_4$ (LFP) nanosheet cathode; (d) cycling performance of the pouch cell under flat, 90° bent, 180° bent, and roll states for 20 cycles, respectively. Reproduced with permission.[218] Copyright 2015, Elsevier. (e) Cycling stability and the coulombic efficiency of LFP and TOT (TOT = LFP+ZFO). (f) Ragone-like plot of $ZnFe_2O_4$/$LiFePO_4$-CNT (ZFO/LFP-CNT) full cells employing anodes with different degrees of lithiation. Reproduced with permission.[220] Copyright 2014, Wiley-VCH.

aid of the synergistic effect between the different components. In addition, other newly developed Zn-based nitrogen and oxygen group compounds with unique physical and chemical properties demonstrate fascinating features as anode candidates for LIBs.

In view of the unclear mechanism of the synergistic effect in increasing the capacity of ZnO and other metal oxide composites, more attention needs to be paid to in-depth mechanism analysis. At present, ZnO electrode performance still can be further enhanced by heteroatom doping and carbon coating, but the major drawbacks are difficulty in determining the optimized additive proportion of heteroatoms or carbon in the ZnO material and realizing uniform doping or coating. A single modification method can only address a partial issue to a certain degree. Combining two or more approaches simultaneously is worth exploring for Zn-based electrodes with satisfactory reversible capacity and cycling stability. The currently developed modification strategies concentrate on promoting the electrochemical performance of the electrodes. Unfortunately, the issues of cost and mass production are commonly ignored. Development of a cost-effective method to

produce high-performance Zn-based electrode materials on a large scale for commercial applications is urgently needed. The solid-phase method may be a potential strategy for the commercialization of ZnO-based anodes because of the facile reaction conditions, low cost, and excellent compatibility with industrial equipment.

Over the past few years, intense research has proved Zn-based nanomaterials to be a promising anode material for LIBs, but there is still a long way to go before real-life application. A series of problems such as cost, initial coulombic efficiency, capacity decay, volumetric energy density, electrical conductivity of materials, and safety should be solved to meet the actual market requirements. In addition, advanced equipment and techniques should also be developed for the nanomaterial systems. Further studies are necessary to determine how nanostructure and morphology can be manipulated to achieve optimal electrochemical performance. And more continuous efforts are required to achieve the final success of Zn-based nanomaterials for next-generation LIBs.

1430 | *Mater. Chem. Front.,* 2018, **2**, 1414–1435

This journal is © The Royal Society of Chemistry and the Chinese Chemical Society 2018

Conflicts of interest

There are no conflicts to declare.

Acknowledgements

References

1 B. Dunn, H. Kamath and J. M. Tarascon, *Science*, 2011, **334**, 928–935.

2 N. Nitta, F. X. Wu, J. T. Lee and G. Yushin, *Mater. Today*, 2015, **18**, 252–264.

3 K. Kang, Y. S. Meng, J. Breger, C. P. Grey and G. Ceder, *Science*, 2006, **311**, 977–980.

4 V. Aravindan, Y. S. Lee and S. Madhavi, *Adv. Energy Mater.*, 2015, **5**, 1402225.

5 Q.-C. Liu, T. Liu, D.-P. Liu, Z.-J. Li, X.-B. Zhang and Y. Zhang, *Adv. Mater.*, 2016, **28**, 8413–8418.

6 G. H. Zhang, Y. Song, H. Zhang, J. Xu, H. G. Duan and J. Y. Liu, *Adv. Funct. Mater.*, 2016, **26**, 3012–3020.

7 J.-J. Xu, Z.-W. Chang, Y.-B. Yin and X.-B. Zhang, *ACS Cent. Sci.*, 2017, **3**, 598–604.

8 K. X. Wang, X. H. Li and J. S. Chen, *Adv. Mater.*, 2015, **27**, 527–545.

9 S. Yuan, Y.-H. Zhu, W. Li, S. Wang, D. Xu, L. Li, Y. Zhang and X.-B. Zhang, *Adv. Mater.*, 2017, **29**, 1602469.

10 L. Wang, G. H. Zhang, X. J. Zhang, H. M. Shi, W. Zeng, H. Zhang, Q. Liu, C. C. Li, Q. H. Liu and H. G. Duan, *J. Mater. Chem. A*, 2017, **5**, 14801–14810.

11 G. M. Zhou, F. Li and H. M. Cheng, *Energy Environ. Sci.*, 2014, **7**, 1307–1338.

12 S. Wang, T. Sun, S. Yuan, Y.-h. Zhu, X.-b. Zhang, J.-m. Yan and Q. Jiang, *Mater. Horiz.*, 2017, **4**, 1122–1127.

13 J. Zhang, H. Ren, J. Wang, J. Qi, R. Yu, D. Wang and Y. Liu, *J. Mater. Chem. A*, 2016, **4**, 17673–17677.

14 W. Liu, M. S. Song, B. Kong and Y. Cui, *Adv. Mater.*, 2017, **29**, 1603436.

15 H. Li, H. Ma, M. Yang, B. Wang, H. Shao, L. Wang, R. Yu and D. Wang, *Mater. Res. Bull.*, 2017, **87**, 224–229.

16 Q. Liu, Z. Chang, Z. Li and X. Zhang, *Small Methods*, 2018, **2**, 1700231.

17 Z. Tang, G. Zhang, H. Zhang, L. Wang, H. Shi, D. Wei and H. Duan, *Energy Storage Mater.*, 2018, **10**, 75–84.

18 J.-J. Xu and X.-B. Zhang, *Nat. Energy*, 2017, **2**, 17133.

19 J. Xu, J. Ma, Q. Fan, S. Guo and S. Dou, *Adv. Mater.*, 2017, **29**, 1606454.

20 L.-P. Wang, N.-W. Li, T.-S. Wang, Y.-X. Yin, Y.-G. Guo and C.-R. Wang, *Electrochim. Acta*, 2017, **244**, 172–177.

21 Z.-D. Huang, Z. Gong, Q. Kang, Y. Fang, X.-S. Yang, R. Liu, X. Lin, X. Feng, Y. Ma and D. Wang, *Mater. Chem. Front.*, 2017, **1**, 1975–1981.

22 M. V. Reddy, G. V. Subba Rao and B. V. Chowdari, *Chem. Rev.*, 2013, **113**, 5364–5457.

23 K. Cao, T. Jin, L. Yang and L. Jiao, *Mater. Chem. Front.*, 2017, **1**, 2213–2242.

24 J. Zhang, P. Gu, J. Xu, H. Xue and H. Pang, *Nanoscale*, 2016, **8**, 18578–18595.

25 Q. Xie, X. Zhang, X. Wu, H. Wu, X. Liu, G. Yue, Y. Yang and D.-L. Peng, *Electrochim. Acta*, 2014, **125**, 659–665.

26 Z. Zhou, K. Zhang, J. Liu, H. Peng and G. Li, *J. Power Sources*, 2015, **285**, 406–412.

27 P. Poizot, S. Laruelle, S. Grugeon, L. Dupont and J. Tarascon, *Nature*, 2000, **407**, 496–499.

28 J. Zhang, T. He, W. Zhang, J. Sheng, I. S. Amiinu, Z. Kou, J. Yang, L. Mai and S. Mu, *Adv. Energy Mater.*, 2017, **7**, 1602092.

29 L. Yu, H. Hu, H. B. Wu and X. W. Lou, *Adv. Mater.*, 2017, **29**, 1604563.

30 J.-Y. Li, Q. Xu, G. Li, Y.-X. Yin, L.-J. Wan and Y.-G. Guo, *Mater. Chem. Front.*, 2017, **1**, 1691–1708.

31 H. Sun, L. Mei, J. Liang, Z. Zhao, C. Lee, H. Fei, M. Ding, J. Lau, M. Li, C. Wang, X. Xu, G. Hao, B. Papandrea, I. Shakir, B. Dunn, Y. Huang and X. Duan, *Science*, 2017, **356**, 599–604.

32 Q. Su, Z. Dong, J. Zhang, G. Du and B. Xu, *Nanotechnology*, 2013, **24**, 255705.

33 M.-G. Park, G.-K. Sung, N.-E. Sung, J.-H. Kim and C.-M. Park, *J. Power Sources*, 2016, **328**, 607–614.

34 H. Li, Y. Wei, Y. Zhang, F. Yin, C. Zhang, G. Wang and Z. Bakenov, *Ionics*, 2016, **22**, 1387–1393.

35 W. H. Shin, T. H. Hwang, Y. S. Huh and J. W. Choi, *J. Electrochem. Soc.*, 2012, **159**, 2143–2147.

36 H. Wang, Q. Pan, Y. Cheng, J. Zhao and G. Yin, *Electrochim. Acta*, 2009, **54**, 2851–2855.

37 S. Kundu, S. Sain, M. Yoshio, T. Kar, N. Gunawardhana and S. K. Pradhan, *Appl. Surf. Sci.*, 2015, **329**, 206–211.

38 A. Kushima, X. H. Liu, G. Zhu, Z. L. Wang, J. Y. Huang and J. Li, *Nano Lett.*, 2011, **11**, 4535–4541.

39 Y. Zhang, Z. Wang, Y. Li and K. Zhao, *Mech. Mater.*, 2015, **91**, 313–322.

40 K. T. Park, F. Xia, S. W. Kim, S. B. Kim, T. Song, U. Paik and W. I. Park, *J. Phys. Chem. C*, 2013, **117**, 1037–1043.

41 H. J. Yang, S. C. Lim, S. Y. He and H. Y. Tuan, *RSC Adv.*, 2015, **5**, 33392–33399.

42 H. Asayesh-Ardakani, W. Yao, Y. Yuan, A. Nie, K. Amine, J. Lu and R. Shahbazian-Yassar, *Small Methods*, 2017, **1**, 1700202.

43 M. Laurenti, N. Garino, S. Porro, M. Fontana and C. Gerbaldi, *J. Alloys Compd.*, 2015, **640**, 321–326.

44 Z.-W. Fu, F. Huang, Y. Zhang, Y. Chu and Q.-Z. Qin, *J. Electrochem. Soc.*, 2003, **150**, 714–720.

45 X. H. Huang, R. Q. Guo, J. B. Wu and P. Zhang, *Mater. Lett.*, 2014, **122**, 82–85.

46 X. Wang, L. Huang, Y. Zhao, Y. Zhang and G. Zhou, *Nanoscale Res. Lett.*, 2016, **11**, 37.

This journal is © The Royal Society of Chemistry and the Chinese Chemical Society 2018

Mater. Chem. Front., 2018, **2**, 1414–1435 | 1431

47 F. Li, L. Yang, G. Xu, H. Xiaoqiang, X. Yang, X. Wei, Z. Ren, G. Shen and G. Han, *J. Alloys Compd.*, 2013, **577**, 663–668.

48 V. Cauda, D. Pugliese, N. Garino, A. Sacco, S. Bianco, F. Bella, A. Lamberti and C. Gerbaldi, *Energy*, 2014, **65**, 639–646.

49 N. Garino, A. Lamberti, R. Gazia, A. Chiodoni and C. Gerbaldi, *J. Alloys Compd.*, 2014, **615**, 454–458.

50 J. Yan, G. Wang, H. Wang, Z. Zhang, X. Ruan, W. Zhao, J. Yun and M. Xu, *J. Nanopart. Res.*, 2015, **17**, 52.

51 G. Yuan, G. Wang, H. Wang and J. Bai, *Ionics*, 2014, **21**, 365–371.

52 L. Xiao, D. Mei, M. Cao, D. Qu and B. Deng, *J. Alloys Compd.*, 2015, **627**, 455–462.

53 J. Wang, H. Tang, H. Wang, R. Yu and D. Wang, *Mater. Chem. Front.*, 2017, **1**, 414–430.

54 C. Xiao, S. Zhang, S. Wang, Y. Xing, R. Lin, X. Wei and W. Wang, *Electrochim. Acta*, 2016, **189**, 245–251.

55 X. Shen, D. Mu, S. Chen, B. Wu and F. Wu, *ACS Appl. Mater. Interfaces*, 2013, **5**, 3118–3125.

56 C. Zhang, Z. Zhang, F. Yin, Y. Zhang, A. Mentbayeva, M.-R. Babaa, A. Molkenova and Z. Bakenov, *ChemElectroChem*, 2017, **4**, 2359–2365.

57 E. Quartarone, V. Dall'Asta, A. Resmini, C. Tealdi, I. G. Tredici, U. A. Tamburini and P. Mustarelli, *J. Power Sources*, 2016, **320**, 314–321.

58 C. Chen, H. Zhang, Y. Xu, M. Ji, H. Dong and C. Zhao, *RSC Adv.*, 2015, **5**, 40219–40226.

59 J. Liu, Y. Li, R. Ding, J. Jiang, Y. Hu, X. Ji, Q. Chi, Z. Zhu and X. Huang, *J. Phys. Chem. C*, 2009, **113**, 5336–5339.

60 S. Lu, H. Wang, J. Zhou, X. Wu and W. Qin, *Nanoscale*, 2017, **9**, 1184–1192.

61 Z. Tu, G. Yang, H. Song and C. Wang, *ACS Appl. Mater. Interfaces*, 2017, **9**, 439–446.

62 Z. Bai, Y. Zhang, N. Fan, C. Guo and B. Tang, *Mater. Lett.*, 2014, **119**, 16–19.

63 G. Z. Yang, H. W. Song, H. Cui, Y. C. Liu and C. X. Wang, *Nano Energy*, 2013, **2**, 579–585.

64 Y. Mao, Q. Wang, X. Wu, H. Xie, X. Ma and M. Chen, *Energy Technol.*, 2018, **6**, 188–195.

65 J. Xu, Y. Dou, Z. Wei, J. Ma, Y. Deng, Y. Li, H. Liu and S. Dou, *Adv. Sci.*, 2017, **4**, 1700146.

66 R. Guo, W. Yue, Y. An, Y. Ren and X. Yan, *Electrochim. Acta*, 2014, **135**, 161–167.

67 M. Yu, A. Wang, Y. Wang, C. Li and G. Shi, *Nanoscale*, 2014, **6**, 11419–11424.

68 C. Kim, J. W. Kim, H. Kim, D. H. Kim, C. Choi, Y. S. Jung and J. Park, *Chem. Mater.*, 2016, **28**, 8498–8503.

69 J. Zheng, J. Lin, R. Chu, C. Wu, J. Zhang, Y. Chen, Y. Zhang and H. Guo, *J. Appl. Electrochem.*, 2017, **47**, 969–978.

70 M. Yu, D. Shao, F. Lu, X. Sun, H. Sun, T. Hu, G. Wang, S. Sawyer, H. Qiu and J. Lian, *Electrochem. Commun.*, 2013, **34**, 312–315.

71 Y. Feng, Y. Zhang, X. Song, Y. Wei and V. S. Battaglia, *Sustainable Energy Fuels*, 2017, **1**, 767–779.

72 S. Li, Y. Xiao, X. Wang and M. Cao, *Phys. Chem. Chem. Phys.*, 2014, **16**, 25846–25853.

73 H. Fang, L. Zhao, W. Yue, Y. Wang, Y. Jiang and Y. Zhang, *Electrochim. Acta*, 2015, **186**, 397–403.

74 C.-T. Hsieh, C.-Y. Lin, Y.-F. Chen and J.-S. Lin, *Electrochim. Acta*, 2013, **111**, 359–365.

75 X. Sun, C. Zhou, M. Xie, H. Sun, T. Hu, F. Lu, S. M. Scott, S. M. George and J. Lian, *J. Mater. Chem. A*, 2014, **2**, 7319–7326.

76 Z. H. Li, X. Yu, Y. Liu, W. X. Zhao, H. Zhang, R. M. Xu, D. H. Wang and H. Shen, *J. Mater. Chem. A*, 2016, **4**, 19123–19131.

77 N. Li, S. X. Jin, Q. Y. Liao and C. X. Wang, *ACS Appl. Mater. Interfaces*, 2014, **6**, 20590–20596.

78 Y. Zhang, Y. Wei, H. Li, Y. Zhao, F. Yin and X. Wang, *Mater. Lett.*, 2016, **184**, 235–238.

79 S. M. Abbas, S. T. Hussain, S. Ali, N. Ahmad, N. Ali and S. Abbas, *J. Mater. Sci.*, 2013, **48**, 5429–5436.

80 Y. Zou, Z. Qi, W. Jiang, J. Duan and Z. Ma, *Mater. Lett.*, 2017, **199**, 57–60.

81 H. Köse, Ş. Karaal, A. O. Aydın and H. Akbulut, *J. Power Sources*, 2015, **295**, 235–245.

82 Y. Zou, Z. Qi, Z. Ma, W. Jiang, R. Hu and J. Duan, *J. Electroanal. Chem.*, 2017, **788**, 184–191.

83 D. Wang, J. Guo, C. Cui, J. Ma and A. Cao, *Mater. Res. Bull.*, 2018, **101**, 305–310.

84 H. Zhang, Y. Wang, W. Zhao, M. Zou, Y. Chen, L. Yang, L. Xu, H. Wu and A. Cao, *ACS Appl. Mater. Interfaces*, 2017, **9**, 37813–37822.

85 L. Shen and C. Wang, *RSC Adv.*, 2015, **5**, 88989–88995.

86 Q. Gan, K. Zhao, S. Liu and Z. He, *Electrochim. Acta*, 2017, **250**, 292–301.

87 Y. Song, Y. Chen, J. Wu, Y. Fu, R. Zhou, S. Chen and L. Wang, *J. Alloys Compd.*, 2017, **694**, 1246–1253.

88 S. Gao, R. Fan, B. Li, L. Qiang and Y. Yang, *Electrochim. Acta*, 2016, **215**, 171–178.

89 Q. Li, H. Zhang, S. Lou, Y. Qu, P. Zuo, Y. Ma, X. Cheng, C. Du, Y. Gao and G. Yin, *Ceram. Int.*, 2017, **43**, 11998–12004.

90 Y. Han, D. Yu, J. Zhou, P. Xu, P. Qi, Q. Wang, S. Li, X. Fu, X. Gao, C. Jiang, X. Feng and B. Wang, *Chemistry*, 2017, **23**, 11513–11518.

91 C. Shi, Y. Gao, L. Liu, Y. Song, X. Wang, H.-J. Liu and Q. Liu, *J. Nanopart. Res.*, 2016, **18**, 371.

92 Y. Zhang, Y. Lu, S. Feng, D. Liu, Z. Ma and S. Wang, *J. Mater. Chem. A*, 2017, **5**, 22512–22518.

93 S. J. Yang, S. Nam, T. Kim, J. H. Im, H. Jung, J. H. Kang, S. Wi, B. Park and C. R. Park, *J. Am. Chem. Soc.*, 2013, **135**, 7394–7397.

94 Y. Han, P. Qi, S. Li, X. Feng, J. Zhou, H. Li, S. Su, X. Li and B. Wang, *Chem. Commun.*, 2014, **50**, 8057–8060.

95 G. Zhang, S. Hou, H. Zhang, W. Zeng, F. Yan, C. C. Li and H. Duan, *Adv. Mater.*, 2015, **27**, 2400–2405.

96 A. Li, H. H. Song, Z. Bian, L. L. Shi, X. H. Chen and J. S. Zhou, *J. Mater. Chem. A*, 2017, **5**, 5934–5942.

97 G. H. An, D. Y. Lee and H. J. Ahn, *ACS Appl. Mater. Interfaces*, 2017, **9**, 12478–12485.

98 G. Zhang, H. Zhang, X. Zhang, W. Zeng, Q. Su, G. Du and H. Duan, *Electrochim. Acta*, 2015, **186**, 165–173.

99 P. Li, Y. Liu, J. Liu, Z. Li, G. Wu and M. Wu, *Chem. Eng. J.*, 2015, **271**, 173–179.

100 H. Fan, H. Yu, Y. Zhang, J. Guo, Z. Wang, H. Wang, X. Hao, N. Zhao, H. Geng, Z. Dai, Q. Yan and J. Xu, *Nano Energy*, 2017, **33**, 168–176.

101 H. Ning, H. Xie, Q. Zhao, J. Liu, W. Tian, Y. Wang and M. Wu, *J. Alloys Compd.*, 2017, **722**, 716–720.

102 Y. Liu, Y. Li, M. Zhong, Y. Hu, P. Hu, M. Zhu, W. Li and Y. Li, *Mater. Lett.*, 2016, **171**, 244–247.

103 F. Sun, J. Gao, H. Wu, X. Liu, L. Wang, X. Pi and Y. Lu, *Carbon*, 2017, **113**, 46–54.

104 S. Y. Kim and B.-H. Kim, *Synth. Met.*, 2015, **210**, 386–391.

105 Z. Ren, Z. Wang, C. Chen, J. Wang, X. Fu, C. Fan and G. Qian, *Electrochim. Acta*, 2014, **146**, 52–59.

106 G. Xia, L. Zhang, F. Fang, D. Sun, Z. Guo, H. Liu and X. Yu, *Adv. Funct. Mater.*, 2016, **26**, 6188–6196.

107 O. B. Chae, S. Park, J. H. Ryu and S. M. Oh, *J. Electrochem. Soc.*, 2012, **160**, 11–14.

108 D. Wei, Z. Xu, J. Wang, Y. Sun, S. Zeng, W. Li and X. Li, *J. Alloys Compd.*, 2017, **714**, 13–19.

109 Y. Li, Y. Zhao, G. Huang, B. Xu, B. Wang, R. Pan, C. Men and Y. Mei, *ACS Appl. Mater. Interfaces*, 2017, **9**, 38522–38529.

110 T. Kim, H. Kim, J.-M. Han and J. Kim, *Electrochim. Acta*, 2017, **253**, 190–199.

111 Y. Hao, S. Wang, J. Zeng, H. Li, P. Yang, B. Liu, S. Zhang and Y. Xing, *Ceram. Int.*, 2018, **44**, 1321–1327.

112 Y. Sun, G. Z. Yang, H. Cui, J. Wang and C. X. Wang, *ACS Appl. Mater. Interfaces*, 2015, **7**, 15230–15239.

113 X. Shen, D. Mu, S. Chen, R. Huang and F. Wu, *J. Mater. Chem. A*, 2014, **2**, 4309–4315.

114 L. Fan, J. Zhang, Y. Zhu and Y. Qian, *Chin. Sci. Bull.*, 2014, **59**, 2006–2011.

115 F. Mueller, D. Geiger, U. Kaiser, S. Passerini and D. Bresser, *ChemElectroChem*, 2016, **3**, 1311–1319.

116 L. Zhang, J. Zhang, Y. Liu, P. Zheng, X. Yuan and S. Guo, *Mater. Lett.*, 2016, **165**, 165–168.

117 J. Duan, S. Yuan, C. Zhu, Z. Chen, G. Zhang, H. Duan, L. Li and Z. Zhu, *Synth. Met.*, 2017, **226**, 39–45.

118 H. Yang, W. Cui, Y. Han and B. Wang, *Chin. Chem. Lett.*, 2017, DOI: 10.1016/j.cclet.2017.09.024.

119 Q. Xie, Y. Ma, X. Zhang, L. Wang, G. Yue and D.-L. Peng, *J. Alloys Compd.*, 2015, **619**, 235–239.

120 M. Ahmad, S. Yingying, A. Nisar, H. Sun, W. Shen, M. Wei and J. Zhu, *J. Mater. Chem.*, 2011, **21**, 7723–7729.

121 H. Yue, Z. Shi, Q. Wang, T. du, Y. Ding, J. Zhang, N. Huo and S. Yang, *RSC Adv.*, 2015, **5**, 75653–75658.

122 Q. Xie, Y. Ma, D. Zeng, X. Zhang, L. Wang, G. Yue and D. L. Peng, *ACS Appl. Mater. Interfaces*, 2014, **6**, 19895–19904.

123 Y. Xiao and M. Cao, *J. Power Sources*, 2016, **305**, 1–9.

124 Q. Xie, L. Lin, Y. Ma, D. Zeng, J. Yang, J. Huang, L. Wang and D.-L. Peng, *Electrochim. Acta*, 2017, **226**, 79–88.

125 L. Wang, K. Tang, M. Zhang and J. Xu, *Nanoscale Res. Lett.*, 2015, **10**, 280.

126 A. K. Giri, P. Pal, R. Ananthakumar, M. Jayachandran, S. Mahanty and A. B. Panda, *Cryst. Growth Des.*, 2014, **14**, 3352–3359.

127 J. Zhao, J. Su, S. Liu, X. Chen, T. Huang and A. Yu, *RSC Adv.*, 2017, **7**, 5459–5465.

128 X. Lu, A. Xie, C. Jiang, M. Lu, Y. Zhang, H. Zhong and S. Zhuang, *RSC Adv.*, 2017, **7**, 4269–4277.

129 Q. Xie, Y. Ma, X. Wang, D. Zeng, L. Wang, L. Mai and D. L. Peng, *ACS Nano*, 2016, **10**, 1283–1291.

130 Y. Wang, X. Jiang, L. Yang, N. Jia and Y. Ding, *ACS Appl. Mater. Interfaces*, 2014, **6**, 1525–1532.

131 H. Yue, Z. Shi, Q. Wang, Z. Cao, H. Dong, Y. Qiao, Y. Yin and S. Yang, *ACS Appl. Mater. Interfaces*, 2014, **6**, 17067–17074.

132 D. Bresser, F. Mueller, M. Fiedler, S. Krueger, R. Kloepsch, D. Baither, M. Winter, E. Paillard and S. Passerini, *Chem. Mater.*, 2013, **25**, 4977–4985.

133 J. Yu, S. Chen, W. Hao and S. Zhang, *ACS Nano*, 2016, **10**, 2500–2508.

134 Y. Feng, R. Zou, D. Xia, L. Liu and X. Wang, *J. Mater. Chem. A*, 2013, **1**, 9654–9658.

135 H. Yan, Y. Luo, X. Xu, L. He, J. Tan, Z. Li, X. Hong, P. He and L. Mai, *ACS Appl. Mater. Interfaces*, 2017, **9**, 27707–27714.

136 L. Liu, C. Zhao, H. Zhao, Q. Zhang and Y. Li, *Electrochim. Acta*, 2014, **135**, 224–231.

137 X. Chen, Y. Huang, X. Zhang, C. Li, J. Chen and K. Wang, *Mater. Lett.*, 2015, **152**, 181–184.

138 Z. Yin, J. Qin, W. Wang and M. Cao, *Nano Energy*, 2017, **31**, 367–376.

139 J. Li, D. Yan, S. Hou, T. Lu, Y. Yao, D. H. C. Chua and L. Pan, *Chem. Eng. J.*, 2018, **335**, 579–589.

140 J. Deng, X. Yu, X. Qin, B. Liu, Y.-B. He, B. Li and F. Kang, *Energy Storage Mater.*, 2018, **11**, 184–190.

141 Q. Pan, L. Qin, J. Liu and H. Wang, *Electrochim. Acta*, 2010, **55**, 5780–5785.

142 Y. Huang, X. Chen, K. Zhang and X. Feng, *Ceram. Int.*, 2015, **41**, 13532–13540.

143 L. Qiao, X. Wang, L. Qiao, X. Sun, X. Li, Y. Zheng and D. He, *Nanoscale*, 2013, **5**, 3037–3042.

144 Q. Xie, Y. Ma, D. Zeng, L. Wang, G. Yue and D. L. Peng, *Sci. Rep.*, 2015, **5**, 8351.

145 M.-S. Wu and H.-W. Chang, *J. Phys. Chem. C*, 2013, **117**, 2590–2599.

146 L. Qin, Q. Zhu, G. Li, F. Liu and Q. Pan, *J. Mater. Chem.*, 2012, **22**, 7544–7550.

147 C. Zhang, J. Dai, P. Zhang, S. Zhang, H. Zhang, Y. Shen and A. Xie, *Ceram. Int.*, 2016, **42**, 1044–1049.

148 L. Luo, W. Xu, Z. Xia, Y. Fei, J. Zhu, C. Chen, Y. Lu, Q. Wei, H. Qiao and X. Zhang, *Ceram. Int.*, 2016, **42**, 10826–10832.

149 H. Köse, Ş. Dombaycıoğlu, A. O. Aydın and H. Akbulut, *Int. J. Hydrogen Energy*, 2016, **41**, 9924–9932.

150 N. Feng, L. Qiao, D. Hu, X. Sun, P. Wang and D. He, *RSC Adv.*, 2013, **3**, 7758–7764.

151 Q. Guo, S. Chen and X. Qin, *Mater. Lett.*, 2014, **128**, 50–53.

152 L. Gao, S. Li, D. Huang, Y. Shen and M. Wang, *Electrochim. Acta*, 2015, **182**, 529–536.

153 S. H. Choi and Y. C. Kang, *Chemistry*, 2014, **20**, 3014–3018.

154 M. S. Song, S. Nahm, W. I. Cho and C. Lee, *Phys. Chem. Chem. Phys.*, 2015, **17**, 23496–23502.

This journal is © The Royal Society of Chemistry and the Chinese Chemical Society 2018

Mater. Chem. Front., 2018, **2**, 1414–1435 | 1433

155 J. Deng, X. Yu, Y. He, B. Li, Q.-H. Yang and F. Kang, *Energy Storage Mater.*, 2017, **6**, 61–69.

156 H.-Q. Dai, H. Xu, Y.-N. Zhou, F. Lu and Z.-W. Fu, *J. Phys. Chem. C*, 2011, **116**, 1519–1525.

157 L. Zhang, T. Wei, J. Yue, L. Sheng, Z. Jiang, D. Yang, L. Yuan and Z. Fan, *J. Mater. Chem. A*, 2017, **5**, 11188–11196.

158 C. Yuan, H. Cao, S. Zhu, H. Hua and L. Hou, *J. Mater. Chem. A*, 2015, **3**, 20389–20398.

159 X. Yang, H. Xue, Q. Yang, R. Yuan, W. Kang and C.-S. Lee, *Chem. Eng. J.*, 2017, **308**, 340–346.

160 J. Li, K. Du, Y. Lai, Y. Chen and Z. Zhang, *J. Mater. Chem. A*, 2017, **5**, 10843–10848.

161 X. Lu, A. Xie, Y. Zhang, H. Zhong, X. Xu, H. Liu and Q. Xie, *Electrochim. Acta*, 2017, **249**, 79–88.

162 D. Cai, H. Zhan and T. Wang, *Mater. Lett.*, 2017, **197**, 241–244.

163 L. Hou, L. Lian, L. Zhang, G. Pang, C. Yuan and X. Zhang, *Adv. Funct. Mater.*, 2015, **25**, 238–246.

164 G. Fang, J. Zhou, Y. Cai, S. Liu, X. Tan, A. Pan and S. Liang, *J. Mater. Chem. A*, 2017, **5**, 13983–13993.

165 B. N. Joshi, S. An, H. S. Jo, K. Y. Song, H. G. Park, S. Hwang, S. S. Al-Deyab, W. Y. Yoon and S. S. Yoon, *ACS Appl. Mater. Interfaces*, 2016, **8**, 9446–9453.

166 L. Lu, H. Y. Wang, J. G. Wang, C. Wang and Q. C. Jiang, *J. Mater. Chem. A*, 2017, **5**, 2530–2538.

167 C. W. Lee, S.-D. Seo, D. W. Kim, S. Park, K. Jin, D.-W. Kim and K. S. Hong, *Nano Res.*, 2013, **6**, 348–355.

168 X. Ge, Z. Li, C. Wang and L. Yin, *ACS Appl. Mater. Interfaces*, 2015, **7**, 26633–26642.

169 Z. Li and L. Yin, *J. Mater. Chem. A*, 2015, **3**, 21569–21577.

170 X. H. Xu, K. Z. Cao, Y. J. Wang and L. F. Jiao, *J. Mater. Chem. A*, 2016, **4**, 6042–6047.

171 M. Jiang, T. Zhou, W. Liu, C. Feng, J. Liu and Z. Guo, *RSC Adv.*, 2017, **7**, 17769–17772.

172 J.-L. Niu, C.-H. Zeng, H.-J. Peng, X.-M. Lin, P. Sathishkumar and Y.-P. Cai, *Small*, 2017, **13**, 1702150.

173 F. Zou, X. Hu, Z. Li, L. Qie, C. Hu, R. Zeng, Y. Jiang and Y. Huang, *Adv. Mater.*, 2014, **26**, 6622–6628.

174 S. Laruelle, S. Grugeon, P. Poizot, M. Dolle, L. Dupont and J. M. Tarascon, *J. Electrochem. Soc.*, 2002, **149**, 627–634.

175 Y.-Y. Hu, Z. Liu, K.-W. Nam, O. J. Borkiewicz, J. Cheng, X. Hua, M. T. Dunstan, X. Yu, K. M. Wiaderek, L.-S. Du, K. W. Chapman, P. J. Chupas, X.-Q. Yang and C. P. Grey, *Nat. Mater.*, 2013, **12**, 1130–1136.

176 J. Wang, H. Tang, L. Zhang, H. Ren, R. Yu, Q. Jin, J. Qi, D. Mao, M. Yang, Y. Wang, P. Liu, Y. Zhang, Y. Wen, L. Gu, G. Ma, Z. Su, Z. Tang, H. Zhao and D. Wang, *Nat. Energy*, 2016, **1**, 16050.

177 M. Keppeler and M. Srinivasan, *ChemElectroChem*, 2017, **4**, 2727–2754.

178 L. He, X.-Z. Liao, K. Yang, Y.-S. He, W. Wen and Z.-F. Ma, *Electrochim. Acta*, 2011, **56**, 1213–1218.

179 M. L. Mao, L. Jiang, L. C. Wu, M. Zhang and T. H. Wang, *J. Mater. Chem. A*, 2015, **3**, 13384–13389.

180 Z. Chen, R. Wu, H. Wang, Y. Jiang, L. Jin, Y. Guo, Y. Song, F. Fang and D. Sun, *Chem. Eng. J.*, 2017, **326**, 680–690.

181 J. Li, Y. Fu, X. Shi, Z. Xu and Z. Zhang, *Chem. – Eur. J*, 2017, **23**, 157–166.

182 Y. Fu, Z. A. Zhang, X. Yang, Y. Q. Gan and W. Chen, *RSC Adv.*, 2015, **5**, 86941–86944.

183 Y. Feng, Y. Zhang, Y. Wei, X. Song, Y. Fu and V. S. Battaglia, *Phys. Chem. Chem. Phys.*, 2016, **18**, 30630–30642.

184 X. Du, H. Zhao, Z. Zhang, Y. Lu, C. Gao, Z. Li, Y. Teng, L. Zhao and K. Świerczek, *Electrochim. Acta*, 2017, **225**, 129–136.

185 X. Du, H. Zhao, Y. Lu, Z. Zhang, A. Kulka and K. Świerczek, *Electrochim. Acta*, 2017, **228**, 100–106.

186 J. B. Li, D. Yan, X. J. Zhang, S. J. Hou, T. Lu, Y. F. Yao and L. K. Pan, *J. Mater. Chem. A*, 2017, **5**, 20428–20438.

187 Z. H. Wang, X. Y. Cao, P. Ge, L. M. Zhu, L. L. Xie, H. S. Hou, X. Q. Qiu and X. B. Ji, *New J. Chem.*, 2017, **41**, 6693–6699.

188 H.-T. Kwon and C.-M. Park, *J. Power Sources*, 2014, **251**, 319–324.

189 Y. Fu, Z. Zhang, K. Du, Y. Qu, Q. Li and X. Yang, *Mater. Lett.*, 2015, **146**, 96–98.

190 Z. Zhang, Y. Fu, X. Yang, Y. Qu and Q. Li, *Electrochim. Acta*, 2015, **168**, 285–291.

191 Z. Chen, R. Wu, H. Wang, K. H. L. Zhang, Y. Song, F. Wu, F. Fang and D. Sun, *Nano Res.*, 2018, **11**, 966–978.

192 Y. Xu, J. Liang, K. Zhang, Y. Zhu, D. Wei and Y. Qian, *Electrochem. Commun.*, 2016, **65**, 44–47.

193 C. M. Park and H. J. Sohn, *Chem. Mater.*, 2008, **20**, 6319–6324.

194 X. Wang, H.-M. Kim, Y. Xiao and Y.-K. Sun, *J. Mater. Chem. A*, 2016, **4**, 14915–14931.

195 M.-P. Bichat, J.-L. Pascal, F. Gillot and F. Favier, *Chem. Mater.*, 2005, **17**, 6761–6771.

196 X. Li, W. Li, J. Yu, H. Zhang, Z. Shi and Z. Guo, *J. Alloys Compd.*, 2017, **724**, 932–939.

197 W. Li, L. Gan, K. Guo, L. Ke, Y. Wei, H. Li, G. Shen and T. Zhai, *Nanoscale*, 2016, **8**, 8666–8672.

198 J.-Y. Chen, L.-C. Chin, G.-A. Li and H.-Y. Tuan, *CrystEngComm*, 2017, **19**, 975–981.

199 S. Saadat, Y. Y. Tay, J. Zhu, P. F. Teh, S. Maleksaeedi, M. M. Shahjamali, M. Shakerzadeh, M. Srinivasan, B. Y. Tay, H. H. Hng, J. Ma and Q. Yan, *Chem. Mater.*, 2011, **23**, 1032–1038.

200 C. M. Park, J. H. Kim, H. Kim and H. J. Sohn, *Chem. Soc. Rev.*, 2010, **39**, 3115–3141.

201 L. Fan, Y. Liu, A. G. Tamirat, Y. Wang and Y. Xia, *New J. Chem.*, 2017, **41**, 13060–13066.

202 M.-G. Park, C. K. Lee and C.-M. Park, *RSC Adv.*, 2014, **4**, 5830–5833.

203 C. M. Park and H. J. Sohn, *Adv. Mater.*, 2010, **22**, 47–52.

204 J. Xu, H. Wu, F. Wang, Y. Xia and G. Zheng, *Adv. Energy Mater.*, 2013, **3**, 286–289.

205 J.-U. Seo and C.-M. Park, *J. Mater. Chem. A*, 2014, **2**, 20075–20082.

206 F. M. Courtel, H. Duncan, Y. Abu-Lebdeh and I. J. Davidson, *J. Mater. Chem.*, 2011, **21**, 10206–10218.

207 H. Duncan, F. M. Courtel and Y. Abu-Lebdeh, *J. Electrochem. Soc.*, 2015, **162**, 7110–7117.

208 H. Rong, Z. Jiang, S. Cheng, B. Chen, Z. Zhen, B. Deng, Y. Qin, G. Xie, Z.-J. Jiang and M. Liu, *RSC Adv.*, 2017, **7**, 18491–18499.

1434 | *Mater. Chem. Front.*, 2018, **2**, 1414–1435

This journal is © The Royal Society of Chemistry and the Chinese Chemical Society 2018

209 J.-H. Lee, M.-H. Hon, Y.-W. Chung and I.-C. Leu, *Appl. Phys. A: Mater. Sci. Process.*, 2010, **102**, 545–550.

210 J. Li, J. Wang, D. Wexler, D. Shi, J. Liang, H. Liu, S. Xiong and Y. Qian, *J. Mater. Chem. A*, 2013, **1**, 15292–15299.

211 R. Zhang, X. Yang, D. Zhang, H. Qiu, Q. Fu, H. Na, Z. Guo, F. Du, G. Chen and Y. Wei, *J. Power Sources*, 2015, **285**, 227–234.

212 J. Fei, Q. Sun, Y. Cui, J. Li and J. Huang, *J. Electroanal. Chem.*, 2017, **804**, 158–164.

213 M.-S. Balogun, W. Qiu, Y. Luo, H. Meng, W. Mai, A. Onasanya, T. K. Olaniyi and Y. Tong, *Nano Res.*, 2016, **9**, 2823–2851.

214 G.-L. Xu, Y. Li, T. Ma, Y. Ren, H.-H. Wang, L. Wang, J. Wen, D. Miller, K. Amine and Z. Chen, *Nano Energy*, 2015, **18**, 253–264.

215 B. Liu, J. Zhang, X. Wang, G. Chen, D. Chen, C. Zhou and G. Shen, *Nano Lett.*, 2012, **12**, 3005–3011.

216 B. Liu, X. Wang, B. Liu, Q. Wang, D. Tan, W. Song, X. Hou, D. Chen and G. Shen, *Nano Res.*, 2013, **6**, 525–534.

217 D. Chen, G. Chen, J. Pei, C. Yan, Y. Hu and Z. Qin, *New J. Chem.*, 2017, **41**, 6973–6976.

218 P. Xiong, L. Peng, D. Chen, Y. Zhao, X. Wang and G. Yu, *Nano Energy*, 2015, **12**, 816–823.

219 J. Xie, W. Song, G. Cao, T. Zhu, X. Zhao and S. Zhang, *RSC Adv.*, 2014, **4**, 7703–7709.

220 A. Varzi, D. Bresser, J. von Zamory, F. Müller and S. Passerini, *Adv. Energy Mater.*, 2014, **4**, 1400054.

221 S. Zhong, H. Zhang, J. Fu, H. Shi, L. Wang, W. Zeng, Q. Liu, G. Zhang and H. Duan, *ChemElectroChem*, 2018, DOI: 10.1002/celc.201800287.

222 D. Wang, W. Zhou, R. Zhang, X. Huang, J. Zeng, Y. Mao, C. Ding, J. Zhang, J. Liu and G. Wen, *J. Mater. Chem. A*, 2018, **6**, 2974–2983.

223 L. Li, S. Liu, H. Zhou, Q. Lei and K. Qian, *Mater. Lett.*, 2018, **216**, 135–138.